Atmos. Meas. Tech. Discuss., 4, 2329–2388, 2011
www.atmos-meas-tech-discuss.net/4/2329/2011/
doi:10.5194/amtd-4-2329-2011

Atmospheric Measurement Techniques Discussions

An improved tropospheric NO_2 column retrieval algorithm for the Ozone Monitoring Instrument

K. F. Boersma[1,2], H. J. Eskes[1], R. J. Dirksen[1], R. J. van der A[1], J. P. Veefkind[1], P. Stammes[1], V. Huijnen[1], Q. L. Kleipool[1], M. Sneep[1], J. Claas[1], J. Leitão[3], A. Richter[3], Y. Zhou[4], and D. Brunner[4]

[1]Royal Netherlands Meteorological Institute, De Bilt, The Netherlands
[2]Eindhoven University of Technology, Eindhoven, The Netherlands
[3]Institute for Environmental Physics, University of Bremen, Bremen, Germany
[4]EMPA, Dübendorf, Switzerland

Received: 15 March 2011 – Accepted: 5 April 2011 – Published: 26 April 2011

Correspondence to: K. F. Boersma (boersma@knmi.nl)

Published by Copernicus Publications on behalf of the European Geosciences Union.

Abstract

We present an improved tropospheric nitrogen dioxide column retrieval algorithm (DOMINO v2.0) for OMI based on better air mass factors (AMFs) and a correction for across-track stripes resulting from calibration errors in the OMI backscattered reflectances. Since October 2004, NO_2 retrievals from the Ozone Monitoring Instrument (OMI), a UV/Vis nadir spectrometer onboard NASA's EOS-Aura satellite, have been used with success in several scientific studies focusing on air quality monitoring, detection of trends, and NO_x emission estimates. Dedicated evaluations of previous DOMINO tropospheric NO_2 retrievals indicated their good quality, but also suggested that the tropospheric columns were susceptible to high biases (by 0–40%), probably because of errors in the air mass factor calculations. Here we update the DOMINO air mass factor approach. We calculate a new look-up table (LUT) for altitude-dependent AMFs based on more realistic atmospheric profile parameters, and include more surface albedo and surface pressure reference points than before. We improve the sampling of the TM4 model, resulting in a priori NO_2 profiles that are better mixed throughout the boundary layer. We evaluate the NO_2 profiles simulated with the improved TM4 sampling as used in the AMF calculations and show that they are highly consistent with in situ NO_2 measurements from aircraft during the INTEX-A and INTEX-B campaigns in 2004 and 2006. Our air mass factor calculations are further updated by the implementation of a high-resolution terrain height and a high-resolution surface albedo climatology based on OMI measurements. Together with a correction for across-track stripes, the overall impact of the improved terrain height and albedo descriptions is modest (<5%) on average over large polluted areas, but still causes significant changes locally. The main changes in the DOMINO v2.0 algorithm follow from the new LUT and the improved TM4 sampling that results in more NO_2 simulated aloft, where sensitivity to NO_2 is higher, and amount to reductions in tropospheric NO_2 columns of up to 20% in winter, and 10% in summer over extended polluted areas. We investigate the impact of aerosols on the NO_2 retrieval, and based on a comparison of concurrent retrievals of

AMTD
4, 2329–2388, 2011

clouds from OMI and aerosols from MODIS Aqua, we find empirical evidence that OMI cloud retrievals are sensitive to the presence of scattering aerosols. It follows that an implicit correction for the effects of aerosols occurs through the aerosol-induced cloud parameters in DOMINO, and we show that such a correction amounts to a 20% AMF reduction in summer and ±10% changes in winter over the eastern US.

1 Introduction

Nitrogen oxides ($NO_x = NO + NO_2$) are released into the atmosphere by anthropogenic and natural sources. These species largely control the production of ozone in the global troposphere (Jacob et al., 1996), and also affect OH concentrations, thereby modifying the residence time of greenhouse gases and other pollutants (e.g. Shindell et al., 2009). The chemical decay product of NO_2, HNO_3, contributes to nitrate aerosol formation (Basset and Seinfeld, 1983) and fertilization of soils and surface waters (Holland and Lamarque, 1997; Michaels et al., 1996). Global mapping of atmospheric NO_2 concentrations can provide important information on NO_x emissions, on the formation of secondary pollutants, as well as on the transport and chemistry of tropospheric nitrogen oxides.

Since the mid-nineties, satellite remote sensing using spectral fitting techniques has been used to derive tropospheric NO_2 concentrations on global, regional, and near-urban scales. Measurements from the Global Ozone Monitoring Experiment (GOME, Burrows et al., 1999) revealed hotspots of air pollution throughout the world (e.g. Leue et al., 2001; Martin et al., 2002), and showed episodes with long-range transport of nitrogen oxides from wildfires (e.g. Spichtinger et al., 2001). Since 2002, retrievals from the Scanning Imaging Spectrometer for Atmospheric Cartography (SCIAMACHY, Bovensmann et al., 1999) have mapped the NO_x pollution in finer spatial detail, and allowed the detection of significant trends in NO_2 concentrations (Richter et al., 2005; van der A et al., 2008). With the launch of the Ozone Monitoring Instrument (OMI, Levelt et al., 2006) in 2004, the spatial detail (up to $13 \times 24\,km^2$) improved to near-urban scales

AMTD
4, 2329–2388, 2011

(Wang et al., 2007; Boersma et al., 2009a). In combination with mid-morning overpasses from SCIAMACHY and GOME-2 (Callies et al., 2000), the 13:40 h overpasses from OMI provide critical information on the timing of NO_x emissions and test our understanding of diurnal NO_x-chemistry (Boersma et al., 2008a, 2009a). In spite of these and many other successful applications of NO_2 satellite measurements, a number of scientific questions about the accuracy of the retrievals remain. As concluded by the community workshop "Tropospheric NO_2 measured by satellites" (September 2007), retrievals should be improved by reducing errors in the air mass factor (AMF), which is the dominant source of error in tropospheric NO_2 retrievals over areas with enhanced NO_2 (Boersma et al., 2004). The AMF defines the relationship between the NO_2 abundance along the average photon path from the Sun through the atmosphere to the satellite (slant column) and the vertical column amount above a certain ground pixel. AMF calculations require external information on atmospheric scattering by air molecules, aerosols, and clouds, the shape of the NO_2 vertical distribution, and on the surface albedo. Current OMI retrievals use AMFs that are calculated with coarse resolution external (forward model) parameters compared to the small OMI pixels (Bucsela et al., 2006; Boersma et al., 2007). This spatial undersampling of the forward model parameters is a source of additional retrieval uncertainties beyond the "classical" error budget as discussed in Boersma et al. (2004).

Here we describe the first major update of the Dutch OMI NO_2 (DOMINO) retrieval algorithm version 1.02 originally described in Boersma et al. (2007) and Boersma et al. (2009b). Data processed with DOMINO v1.02 were released in 2008. Since then, dedicated validation activities and model comparisons brought a number of DOMINO retrieval weaknesses to light. Table 1 summarizes the outcome of the comparisons, bearing in mind that the independent data used for the comparisons was imperfect. The independent data listed in Table 1 struggle with measurement errors and rely (amongst others) on assumptions on boundary layer thickness, vertical mixing, and spatial representativity. Even so, the table shows that DOMINO v1.02 generally agrees well with independent data, but appears to be biased high by 0–40%. The only study

AMTD
4, 2329–2388, 2011

that suggested a possible seasonally dependent bias in the OMI retrievals was by Huijnen et al. (2010), who found good agreement between tropospheric NO_2 from DOMINO v1.02 and regional chemistry transport models in winter, but reported that DOMINO tropospheric NO_2 was much higher than model simulations in summer. In contrast, Lamsal et al. (2010) found that DOMINO v1.02 captures the seasonal variation in tropospheric NO_2 over the US well. Most studies cited in Table 1 made recommendations on how to improve the AMF calculations. In the DOMINO upgrade described here, we improve AMFs by better radiative transfer modelling, more accurate, higher-resolution descriptions of surface albedo and surface pressure, and using more realistic a priori vertical distributions of NO_2. Following on our earlier work (Boersma et al., 2004), we investigate the effect of aerosols in cloud-free scenes on the OMI O_2-O_2 retrievals. This is important because O_2-O_2-retrieved cloud parameters are used to correct for cloud effects in the DOMINO NO_2 retrieval.

It is unlikely that the separation of stratospheric and tropospheric NO_2 slant columns leads to systematic, large-scale biases in the DOMINO tropospheric NO_2 columns. A recent evaluation of the DOMINO stratosphere-troposphere separation scheme indicated that OMI stratospheric NO_2 columns agree well with independent, ground-based measurements (Dirksen et al., 2011). However, DOMINO version 1.02 tropospheric NO_2 columns do show a persistent, stripe-like pattern that indicates an across-track bias. This bias is caused by small jumps in the solar irradiance spectra due to measurement noise and wavelength calibration that are different from one OMI viewing angle to the other. In this study we will also describe and implement a simple method to correct for the across-track bias, but our main concern will be the improved calculation of the OMI NO_2 AMF.

AMTD
4, 2329–2388, 2011

2 OMI tropospheric NO_2 retrieval

2.1 Ozone Monitoring Instrument (OMI)

OMI is the Dutch-Finnish UV-Vis spectrometer on NASA's EOS-Aura satellite. Aura was launched on 15 July 2004 into a Sun-synchronous orbit with a local equator crossing time of approximately 13:40 h. Within the UV-Vis window that ranges from 270–500 nm, OMI detects direct and atmospheric backscattered sunlight. Two-dimensional CCD detectors are used to simultaneously record (ir)radiance spectra for 60 individual satellite viewing angles (rows). The dimensions of the ground pixels are 13–26 km along track and 24–128 km across track depending on the satellite viewing angle. Current scientific data products from OMI are based on Collection 3 level 1b data. Collection 3 data has been better calibrated than previous level 1 data versions (Dobber et al., 2008), although retrievals of minor trace gases based on Collection 3 spectra have shown spurious across-track variability, or stripes, since launch. This situation has deteriorated on 25 June 2007. From that date onwards, OMI has been affected by a number of so-called row anomalies that appear as signal suppressions in the level 1 radiance spectra for particular satellite viewing angles over the complete illuminated orbit. On 1 January 2011, 29 of the 60 rows were (partially) affected. The origin of these anomalies is currently unknown. Until a satisfying correction for these row anomalies has been implemented, data from rows affected by the anomalies should not be used (see e.g. http://www.knmi.nl/omi/research/calibration/instrument_status_v3/index.html). On the other hand, OMI's radiometric stability is very good for a UV-Vis spectrometer. The optical degradation in the visible channel is less than 2% over the period 2004–2010, and together with the good instrument performance, the OMI science data are generally considered to be of high quality for the full 6 year period of the mission thusfar.

AMTD
4, 2329–2388, 2011

2.2 DOMINO retrieval algorithm

The Dutch OMI NO_2 retrieval algorithm consists of three steps: (1) using Differential Optical Absorption Spectroscopy (DOAS) to obtain NO_2 slant columns from the OMI reflectance spectra (Boersma et al., 2002, 2007; Bucsela et al., 2006), (2) separating the stratospheric and tropospheric contribution to the slant column (Boersma et al., 2007; Dirksen et al., 2011), and (3) converting the tropospheric slant column to a vertical column with the tropospheric air mass factor (AMF). These principles are the same in the previous v1.02 algorithm and in the improved retrieval presented here, and they have been described in more detail elsewhere (Boersma et al., 2007, 2009b).

We chose a wide fitting window of 405–465 nm for the spectral fitting of NO_2 in order to compensate for OMIs moderate signal-to-noise ratio compared to other sensors. The absorption cross sections of NO_2, ozone, H_2O, as well as a synthetic Ring spectrum, are fitted to the satellite reflectance spectra. A fifth order polynomial is included in the fit to account for scattering effects. Annual average irradiance measurements for the year 2005 are used as reference for the reflectance spectra. The uncertainty in individual retrievals due to spectral fitting is 0.7×10^{15} molecules cm^{-2} and dominates the overall retrieval error over the oceans and remote areas (Boersma et al., 2007). The NASA Standard Product retrieval (Bucsela et al., 2006) uses the same OMI NO_2 slant columns as the DOMINO retrievals discussed here.

In the second retrieval step, the stratospheric contribution is separated from the total slant column. The stratospheric NO_2 slant column is estimated by assimilating OMI total slant columns in the TM4 chemistry-transport model (Dentener et al., 2003; Boersma et al., 2007). The average (annual) differences between stratospheric NO_2 columns from DOMINO and independent, ground-based techniques were recently shown to be smaller than 0.3×10^{15} molecules cm^{-2} (Dirksen et al., 2011).

AMTD
4, 2329–2388, 2011

The third retrieval step is the focus of this paper. We apply the tropospheric AMF formulation of Palmer et al. (2001) and Boersma et al. (2004) to convert the resulting tropospheric slant columns into vertical columns. Because the slant optical thickness of NO_2 is generally < 0.005, the AMF can be written as the linear sum of atmospheric layer contributions to the slant column ratioed by the vertical column:

$$M = \frac{\sum_l m_l(\hat{\boldsymbol{b}})\, x_{a,l}}{\sum_l x_{a,l}} \quad (1)$$

with m_l the altitude-dependent AMFs that describe the vertically resolved sensitivity to NO_2, and $x_{a,l}$ the layer specific subcolumns from the a priori profile $\boldsymbol{x}_a$ for atmospheric layer l. The altitude-dependent air mass factors are calculated by adding a finite amount of NO_2 to layer l and subsequently ratioing the NO_2 slant column (simulated with a radiative transfer model) to the vertical column added to that layer ($m_l = \partial N_s / \partial x_l$, see Eskes and Boersma, 2003 for more detail). As radiative transfer model we use the Doubling Adding KNMI (DAK) model (Stammes, 2001) version 3.0. The altitude-dependent air mass factors are stored in a look-up table as a function of forward model parameters $\hat{\boldsymbol{b}}$, including the satellite viewing geometry, surface pressure and albedo. Pixel-specific altitude-dependent air mass factors are obtained by using the best estimates for forward model parameters $\hat{\boldsymbol{b}}$, and an interpolation scheme. The previous DOMINO dataset (v1.02) uses a priori NO_2 profiles based on the TM4 assimilation run at a resolution of $2^\circ \times 3^\circ$ (lat × lon) and 35 vertical levels up to 0.38 hPa and spatially interpolated to the OMI pixel center. Similarly, DOMINO v1.02 uses interpolated surface pressures from the $2^\circ \times 3^\circ$ TM4 model, which is driven by operational meteorological fields from ECMWF. Surface albedo information in v1.02 is from the combined $1^\circ \times 1.25^\circ$ TOMS/GOME climatologies (Boersma et al., 2004) for the period October 2004 to February 2009. From 17 February 2009 onwards, the DOMINO v1.02 retrievals were based on the surface albedo from the $0.5^\circ \times 0.5^\circ$ OMI climatology (Kleipool et al., 2008), but the impact of this update on AMFs has not yet been studied. Any changes in the AMF are important to data users because such changes affect the

AMTD
4, 2329–2388, 2011

altitude-dependent air mass factors (m_l), and these, combined with the a priori NO_2 profile, determine the averaging kernel (Eskes and Boersma, 2003), which is provided in the data product.

The AMF formulation accounts for cloud-contaminated pixels. Following Martin et al. (2002) and Boersma et al. (2002), we use the independent pixel approximation to express the AMF as a linear combination of a clear-sky AMF and a cloudy AMF:

$$M = w\,M_{cl} + (1 - w)\,M_{cr} \quad (2)$$

with w the cloud radiance fraction that depends on the effective cloud fraction ($w = f_{cl}\,I_{cl}/R$ with I_{cl} the radiance from the cloud part of the pixel, and R the total scene radiance), and M_{cl} and M_{cr} signifying the cloudy-sky and clear-sky AMFs, respectively. Our AMF calculation uses the effective cloud fraction and cloud pressure from the OMI O_2-O_2 retrieval (OMCLDO2, Acarreta et al., 2004). The O_2-O_2 retrieval is consistent with the NO_2 retrieval in the sense that both use the independent pixel approximation which represents clouds as opaque Lambertian surfaces of albedo 0.8.

AMFs are very sensitive to assumed surface albedo. Clear-sky AMFs (M_{cr}) increase with increasing surface albedo (Boersma et al., 2004). Cloudy-sky AMFs (M_{cl}) depend on the assumed albedo of 0.8 for the Lambertian reflector, but they are independent of the assumed surface albedo. Because the radiance-weighted cloud fractions w decrease with increasing surface albedo, the magnitude of the effect of changes in surface albedo on the AMF is difficult to predict. We will investigate this issue further in Sect. 3.3 where we discuss the direct (clear-sky) and indirect (partly cloudy) impact of improved OMI surface albedos (Kleipool et al., 2008) on the DOMINO retrievals.

3 Improved DOMINO AMF calculations for v2.0

Here we focus on improving four different aspects of the DOMINO air mass factors: the improved (1) radiative transfer calculations, (2) terrain heights, (3) surface albedo, and (4) sampling of the TM4 model. All these are important aspects by themselves, and

AMTD
4, 2329–2388, 2011

we will discuss the effects of the improvements on the retrieval separately. Section 5 discusses the combined effect of all improvements on v2.0 together.

3.1 Altitude-dependent AMFs

Retrieving tropospheric NO_2 columns from solar backscatter observations requires information about the vertical sensitivity to NO_2, or the averaging kernel. These sensitivities, expressed as altitude-dependent AMFs for both clear and cloudy parts of the pixel, are calculated with the DAK radiative transfer model. The DAK model atmosphere consists of a Lambertian surface albedo, and 24 atmospheric layers. Atmospheric data are from the standard AFGL midlatitude summer profile. We calculate the AMF at 439 nm, in the middle of the spectral fitting window for the corresponding OMI NO_2 slant column retrievals. Using a midlatitude winter atmosphere profile (p, T) instead of a summer profile would change the tropospheric AMFs by 1%. Our calculations have been done with a plane parallel version of DAK that accounts for polarization. This is consistent with DAK settings in retrievals of cloud properties and surface albedo from OMI (Acarreta et al., 2004; Kleipool et al., 2008). Although polarization is accounted for, its impact is small, and reduces tropospheric AMFs by $< 0.5\%$ and affects stratospheric retrievals by $< 0.1\%$.

The altitude-dependent AMFs are stored in a look-up table (LUT) as a function of solar zenith angle, viewing zenith angle, relative azimuth angle, Lambertian surface albedo, surface pressure, and (midlevel) atmospheric pressure. Compared to earlier versions of our AMF LUT used in OMI NO_2 retrievals, we extend here the set of surface albedo (from 10 to 16) and surface pressure (from 10 to 15) reference points in the LUT, and include a more realistic pressure and temperature profile. In addition, we eliminate an interpolation error in calculating the altitude-dependent AMF from the LUT for the lowest layer, as suggested by Zhou et al. (2009). For any (TM4) pressure level, the altitude-dependent AMF is found by interpolating between the LUT-values at the two adjacent reference pressure levels. For reference pressure levels exceeding the actual (TM4) surface pressure, the altitude-dependent AMF was assigned a value

AMTD
4, 2329–2388, 2011

of zero (assuming that the sensitivity to below-surface NO_2 is zero). This led to too low (interpolated) altitude-dependent AMFs for the lowest TM4 model layer. By extrapolating the higher-layer AMF curve downward, we now avoid interpolation and obtain more realistic altitude-dependent AMFs for the lowest model layer.

Figure 1 shows the global distribution of the monthly mean January and July 2005 tropospheric AMF for OMI NO_2 calculated with the old (v1.02, left panels) and new AMF LUT (middle panels) for clear-sky situations (cloud radiance fraction < 50%). The AMFs are smallest over polluted regions indicating reduced sensitivity to NO_2 in the boundary layer. AMFs are relatively high over areas with high surface albedo (e.g. the Alps and much of Mongolia in January 2005) and over the oceans where the larger fraction of NO_2 is in the free troposphere. Over polluted regions, tropospheric AMFs with the new LUT are larger by 20–30% (January) and 10–15% (July), leading to reductions in tropospheric NO_2 columns of 20% (January) and 10% (July) over North America, Europe, and eastern Asia. Over snow-covered terrain, AMFs increase by up to 100%, but the reduction in NO_2 columns is marginal over these mostly clean regions. The AMF increases are smaller in July than in January because of the increase in mixing and depth of the boundary layer, reducing the relative importance of downward extrapolation for the lowest layers.

3.2 Terrain height

The AMF calculation also requires local information about the surface pressure. In earlier retrievals this information was obtained from the coarse-resolution ($2^\circ \times 3^\circ$) TM4 model, driven by ECMWF meteorological data. Here we follow the approach presented by Zhou et al. (2009), and take more accurate surface pressures based on Global 3km Digital Elevation Model data (DEM_3km), an Earth Science Data type routinely provided with EOS-Aura data. We convert the coarse-resolution TM4 surface pressure by applying the hypsometric equation and the assumption that temperature changes linearly with height, which is often used for reducing measured surface pressures to sea level (Wallace and Hobbs, 1977):

AMTD
4, 2329–2388, 2011

$$p_{\mathrm{DEM}} = p_{\mathrm{TM4}} \left(\frac{T_{\mathrm{surf}}}{(T_{\mathrm{surf}} + \Gamma\,(h_{\mathrm{TM4}} - h_{\mathrm{DEM}}))} \right)^{-g/R\,\Gamma} \quad (3)$$

where p_{TM4}, T_{surf} are the TM4 surface pressure and temperature, $\Gamma = 6.5\,\mathrm{K\,km^{-1}}$ the lapse rate, h_{TM4} the TM4 terrain height, and h_{DEM} the 3km-resolution terrain height according to the DEM_3km database. $R = 287\,\mathrm{J\,kg^{-1}\,K^{-1}}$ is the gas constant for dry air, and $g = 9.8\,\mathrm{m\,s^{-2}}$ the gravitional constant. For the improved retrieval, the pressure levels for the a priori NO_2 profiles are based on the improved surface pressure level p_{DEM} (with $p_i = a_i + b_i \cdot p_{\mathrm{DEM}}$ and a_i, b_i ECMWF constants that effectively define the vertical coordinate), so that mixing ratios are conserved.

Figure 2 (upper panel) shows the absolute difference between the new high-resolution terrain heights and the coarse TM4 (v1.02) terrain heights for July 2005. Over regions with pronounced orography, the smooth TM4 terrain heights underestimate the elevation of the highest mountains and overestimate the elevation of adjacent valleys, illustrated by marked transitions from red to blue. The improved terrain heights have marginal effect on the retrieved clear-sky (cloud radiance < 50%) NO_2 columns for regions with little pollution or small differences in effective terrain heights as shown in the middle (January 2005) and bottom (July 2005) panels of Fig. 2. Averaged over the polluted regions extended over North America, Europe, and eastern Asia, the change in tropospheric NO_2 columns is within 1% for January and July 2005 (Table 2). Locally the effects can be much stronger. Correcting for overestimated terrain heights leads to increased NO_2 columns (e.g. Po Valley, Tehran), by reducing the – previously too high – AMF. Correcting for underestimated terrain height leads to increased AMFs (sensitivity to for NO_2 at higher altitude is higher) and reduced NO_2 columns (e.g. Mexico City, Highveld area). A net increase in terrain height by 30 m for the polluted Los Angeles area reduces NO_2 columns by 4% during January and July 2005. Net decreases in terrain height by approximately 450 m over the Po Valley and Beijing areas lead to columns that are higher by 12–14% in January and by 3% in July 2005 (Table 3). The impact of improved terrain heights is stronger in winter than in summer, mainly

AMTD
4, 2329–2388, 2011

reflecting the stronger sensitivity to errors in the surface pressure for situations with shallow boundary layers when most NO_2 is concentrated near the surface.

3.3 Surface albedo

AMFs are affected by the surface albedo both directly and via the cloud retrieval. Both these aspects need to be considered when implementing an improved surface albedo climatology in the NO_2 retrieval. In previous OMI retrievals at KNMI, both cloud retrievals (Stammes et al., 2008) and NO_2 AMF calculations used surface albedos from Lambert Equivalent Reflectance, or LER, data sets based on TOMS and GOME measurements. These estimates are limited by the spatial resolution of the TOMS ($1^\circ \times 1.25^\circ$) and GOME ($1^\circ \times 1^\circ$) climatologies. Kleipool et al. (2008) recently developed a surface albedo climatology using three years of OMI data with improved spatial resolution ($0.5^\circ \times 0.5^\circ$). The higher spatial resolution of the OMI reflectance dataset reduces cloud contamination in the surface albedo compared to TOMS/GOME. Another major advantage of the Kleipool et al. (2008) climatology is that either the mode (most frequently observed value) or the 1% cumulative probability threshold of the LER distribution has been used instead of the minimum LER as in the TOMS and GOME climatologies. Because of transient effects, like ground and cloud shading, and darkening by incidental precipitation, the minimum LER is likely to underestimate the overall albedo of a scene. Furthermore, the Kleipool et al. (2008) climatology represents the surface albedo at approximately 13:40 LT (local time), consistent with the OMI observations. Using the OMI albedo climatology for OMI NO_2 retrievals also reduces errors arising from unaddressed instrumental effects and long term trends associated with TOMS/GOME but not with OMI. Furthermore it ensures that the optimal LER is derived under the same illumination conditions (solar zenith angle) so that Bidirectional Reflectance Distribution Function (BRDF) effects are reduced.

AMTD
4, 2329–2388, 2011

3.3.1 Effect of surface albedo changes on OMI cloud parameters

Figure 3 (left panels) shows the monthly mean difference in surface albedo between the OMI (479.5 nm) and the TOMS/GOME (477 nm) climatologies for January and July 2005. Scenes flagged as covered by snow or ice in the OMI data have been excluded. Large negative differences occur over regions where the GOME climatology most likely suffered from contamination by residual cloud or snow/ice. This is observed, for instance, over tropical rain forests in the case of clouds (January and July), and over the northern parts of North America, in the Rhine Valley, and interior China in case of snow (January). For these regions, the TOMS/GOME data set is more likely to report contaminated and therefore higher surface albedos, because of the larger GOME pixels and smaller data volume analysed than in the case of OMI. Surface albedo's for other regions over land are mostly higher in the OMI LER climatology due to the selection of the mode rather than the minimum LER. On average, the albedo differences between OMI and TOMS/GOME (477 nm) in the 60° S to 60° N region are within 0.001 with a standard deviation smaller than 0.012 (see Table 4).

Retrieved cloud parameters are sensitive to changes in the assumed surface albedo. The right panels of Fig. 3 illustrate that for regions with higher surface albedo (e.g. Sahara, Arabian Peninsula), O_2-O_2-retrieved effective cloud fractions are reduced by up to 20%, and vice versa, for regions with lower surface reflectivity (e.g. South America). For the days 1 January and 1 July 2005 (and averaging over all retrieval scenes) the change in effective cloud fraction Δf_{cl} depends on the change in the (477 nm) surface albedo approximately as $\Delta f_{cl} = -0.6\Delta a_{sf}$ (not shown), consistent with theoretical predictions by Koelemeijer et al. (2001). Using the OMI surface albedo climatology leads to a smaller global mean effective cloud fraction (0.303 instead of 0.309), and increases the number of pixels with cloud radiance fractions below 0.5 by 0.5%.

O_2-O_2 cloud pressures are also sensitive to changes in the surface albedo, in particular when the effective cloud fractions are small. For retrievals with low cloud fractions (cloud radiance fractions < 0.5, of most interest for our retrievals), we found that using

AMTD
4, 2329–2388, 2011

the OMI climatology results, on average, in cloud pressures that are lower (by less than −5 hPa) when compared to those resulting from using the TOMS/GOME climatology. The small decrease in average cloud pressures is consistent with the small decrease in average effective cloud fractions (less than −0.006 for both months), because the same strength of the observed spectral O_2-O_2 features needs to be explained by the cloud algorithm (e.g. Acarreta et al., 2004). We find that for situations with low cloud fractions (between 0.05 and 0.20), the change in effective cloud pressure approximately depends on the change in surface albedo as $\Delta p_{cl} = -1400 \Delta a_{sf}$ hPa (an albedo increase of +0.01 leads to cloud pressures reduced by 14 hPa).

3.3.2 Effect of surface albedo changes on NO_2 retrievals

The left panels in Fig. 4 show the absolute differences between the OMI and TOMS/GOME (v1.02) surface albedo climatologies (440 nm) used in the clear-sky AMF calculations for January and July 2005. Scenes flagged as covered by snow or ice in the OMI data have been excluded. The differences between the 440 nm albedos are broadly consistent with those at 479 nm shown in Fig. 3. One exception is the larger difference for desert areas where the increase at 479 nm is stronger than at 440 nm, which can be explained by the significant increase in albedo as a function of wavelength over deserts (e.g. Kleipool et al., 2008). Similar to 479 nm, we see large negative differences over areas that were contaminated by clouds or snow/ice in the the TOMS/GOME climatology. Over land (with the exception of rainforests), the OMI climatology generally reports somewhat higher values than the TOMS/GOME set. On average, the differences between OMI and TOMS/GOME (440 nm) between 60° S and 60° N are within 0.002 with a standard deviation smaller than 0.013 (see Table 5).

From the right panels in Fig. 4 we see that the change in albedo has a negligible effect on the retrieved NO_2 columns for regions with little pollution. The effects of the improved albedo are best seen over the polluted areas of the Northern Hemisphere in winter, when the NO_2 lifetime is longest. Reductions in the 440 nm albedo generally lead to increases in retrieved NO_2 (northeastern US, Europe). Vice versa, over polluted

AMTD
4, 2329–2388, 2011

areas with increased albedo, we see a distinct reduction in NO_2 (southern US, Spain, sub-Saharan Africa). Over northeastern China, the strong reduction in retrieved NO_2 is not accompanied by an increase in the 440 nm albedo. There, the reduction reflects the considerable increase in effective cloud fraction (+0.02) together with a significant increase (+23 hPa) in cloud pressures that are already high (~900 hPa) over this area. These relatively high cloud fractions and pressures may be indicative of large amounts of aerosols in the polluted boundary layer, as we will see in Sect. 6. Higher cloud fractions and higher cloud pressures imply increased sensitivity to NO_2 when the effective cloud pressure is situated within the polluted layer (e.g. Fig. 5a and b in Boersma et al. (2004)). Averaged over the polluted regions of the Northern Hemisphere, the change in tropospheric NO_2 columns due to the improved surface albedo is within 10% in January 2005 and within 3% in July 2005 (see Table 2). The choice for albedo matters most in winter, because in that season most NO_2 is confined in a thin layer near the surface where the satellite vertical sensitivity depends strongest on albedo.

For the polluted hotspots Los Angeles (LA), the Po Valley, and Beijing, albedo changes are stronger than albedo changes averaged over larger polluted areas. Consequently, the effects on retrieved NO_2 are stronger (see Table 3): significant increases in albedo over LA (January: +0.023, July: +0.027) lead to 15% reductions in retrieved NO_2, mostly reflecting increased clear-sky AMFs. In contrast, the reduced albedo over the Po Valley in January (−0.032) leads to a 10% increase in NO_2. Similar to the situation over eastern China, the reduction in NO_2 over Beijing in winter is largely attributed to a significant increase in cloud fraction (from 0.04 to 0.08) and in cloud pressure (from 928 to 950 hPa).

3.4 A priori vertical profiles

Previous studies (Hains et al., 2010; Huijnen et al., 2010) suggested that TM4 NO_2 profiles in polluted regions possibly suffer from too weak mixing in the lowest few model layers. A critical review of the TM4 output module pointed out that upon sampling the TM4 tracer field at 13:30 LT, emissions, chemistry, deposition and vertical transport

AMTD
4, 2329–2388, 2011

all have operated on NO_x, but only the first two have operated on NO_2. In the TM4 model, the chemistry step computes NO_2 from NO_x, but prior to deposition and vertical transport. The resulting 30-min "lag" in the vertical redistribution of NO_2 leads to profiles with artificially strong NO_2 concentrations in the lowest model layers and, consequently, with too little vertical NO_2 transport. By explicitly propagating NO_2 (as well as NO, NO_3, N_2O_5, and HNO_4) as tracers in TM4, we now ensure appropriate sampling of the NO_2 field, i.e. after NO_2 has been subject to deposition and convection.

Figure 5 shows a comparison between TM4 vertical NO_2 profiles simulated for January 2005 (blue) and July 2005 (red) over the US. We see that the high surface layer concentrations in the original simulations (v1.02, dashed lines) are significantly reduced by the simulations with NO_2 as transported tracer in the model. These improvements are most prominent in Summer, when vertical transport is stronger than in winter, resulting in better mixed vertical distributions of NO_2 in that season.

We evaluate the improved TM4 vertical profiles of NO_2 at 13:30 LT used as a priori in the AMF calculation. We compare to vertical NO_2 profiles observed from NASA's DC-8 aircraft during the INTEX-A (July–August 2004) and INTEX-B (March 2006) field campaigns. The flight conditions during these campaigns ranged from remote marine to highly polluted. During INTEX-A, the DC-8 sampled tropospheric air over the eastern US and the North Atlantic Ocean. NOAA's WP-3D also flew over the polluted east coast of North America and over the North Atlantic Ocean (ICARTT campaign). During INTEX-B, the DC-8 sampled the troposphere over the southern US, and (the Gulf of) Mexico. NO_2 was measured from the DC-8 by laser induced fluorescence (Thornton et al., 2000) with 0.02–0.05 ppb precision (for 1-s measurements), and from the WP-3D by chemiluminescence (Ryerson et al. , 2000) during ICARTT with a precision of 0.025 ppbv for the 1-Hz data at low values of NO_2.

Figure 6 compares NO_2 profile shapes simulated by TM4 to those observed from aircraft during the INTEX-A/ICARTT and INTEX-B campaigns. The TM4 simulations are sampled at 13:30 LT, nearly coinciding with the OMI overpass time, and consistent with our AMF calculation. All aircraft observations within three hours of the model

AMTD
4, 2329–2388, 2011

sampling time have been selected. Aircraft measurements and model simulations for the INTEX-A/ICARTT campaign are generally highly consistent throughout the lower troposphere, but the model simulations underestimate NO_2 in the upper troposphere by 0.1 ppb. This is likely due to an underestimate in mid-latitude lightning NO_x production reported earlier by Martin et al. (2006). During INTEX-B, we find reasonable agreement between TM4 and the DC-8 observations for the southern US and Mexico, and very good agreement over the Gulf of Mexico.

The TM4 simulation with NO_2 propagated is in somewhat better agreement with the observations than the original simulation, especially for the southern US, although the largest improvements are found below the aircraft bottom altitude of 150–300 m above surface (see Fig. 5). The underestimation by TM4 of NO_2 over Mexico (0.1 ppb), reflects too low NO_x emissions from the POET inventory (1997) for that area. POET NO_x emissions are consistent with GEIA emissions (1999) that underestimate recently updated estimates from the Mexico National Emissions Inventory by a factor 1.6–1.8 (Boersma et al., 2008a). The AMFs calculated from the observed profiles are generally within 15% of the AMFs calculated from simulated profiles (Hains et al., 2010). Our comparison suggests that boundary layer mixing in TM4, simulated with a non-local scheme, is vigorous enough to appropriately simulate vertical distributions of NO_2. The non-local scheme used in TM4 (Holtslag and Boville, 1993) has recently also been implemented in the GEOS-Chem CTM, which resulted in significantly improved simulations of vertical distributions for NO_2 and O_3 in that model (Lin and McElroy, 2010), and further supports using "non-local" mixing schemes for vertical tracer transport as in TM4.

Figure 7 shows the effect of the improved tropospheric air mass factors on OMI NO_2 retrievals for January and July 2005. We see that, in both seasons, the improved simulations of NO_2 profiles lead to reductions of more than 1.0×10^{15} molec cm^{-2} over regions with strong NO_x emissions. These reductions are due to increases in the tropospheric AMFs that reflect generally higher NO_2 concentrations aloft in our improved TM4 simulations. The impact of the improved TM4 profiles is strongest in summer,

AMTD
4, 2329–2388, 2011

when vertical transport is stronger than in winter. This is reflected by Fig. 5 showing a larger difference between the original and improved TM4 simulation in July than in January 2005. In winter, we see small increases ($<0.5 \times 10^{15}$ molec cm^{-2}) over regions such as rural France and the Midwest of US, reflecting more efficient outflow towards these regions from the adjacent pollution hotspots in TM4. In summer, this effect is negligible because the NO_2 lifetime is too short for NO_x to be transported in significant amounts to these regions. Averaged over the polluted regions of the Northern Hemisphere, the change in tropospheric NO_2 columns due to the improved TM4 NO_2 profiles is within −4% in January 2005 and within −6% in July 2005 (see Table 2). For the polluted hotspots Los Angeles, the Po Valley, and Beijing, the effects of the improved TM4 sampling are somewhat stronger than averaged over the larger polluted areas (approximately −5% and −8% in January and July 2005, respectively). The changes in TM4 NO_2 profiles directly affect the retrieved NO_2 columns, but model-retrieval comparisons using the averaging kernel will not be affected by changes in the TM4 NO_2 profiles, because in such comparisons, the dependence on the a priori (TM4) NO_2 profile cancels (Eskes and Boersma, 2003; Boersma et al., 2004).

4 Destriping

Since its launch in 2004, OMI retrievals have been suffering from spurious across-track variability, or stripes. Recent improvements in the calibration and data processing of the level 1b fields (Collection 3; Dobber et al., 2008) have suppressed striping, and further reductions have been achieved by using the annual average solar irradiance spectrum (2005) instead of individual, daily irradiance measurements for level 1 to 2 retrievals. But even after these improvements, OMI NO_2 retrievals still show some degree of striping. Here we use a simple method to remove the across-track bias in the OMI NO_2 slant columns.

OMI NO_2 slant columns are derived from fitting modeled spectra to observed reflectance spectra in the 405–465 nm window. The reflectance spectra are defined

AMTD
4, 2329–2388, 2011

as the ratio of OMI radiance to the annual average irradiance spectra. For OMI, the spectral fit uses 60 independently observed irradiance spectra as the reference for the along-track radiance measurements. But even after averaging over a complete year, the OMI irradiance measurements for each of the 60 satellite viewing angles still have slightly different levels of noise. In combination with small differences in wavelength calibration for each of the 60 angles, this causes small, but systematic jumps in the top-of-atmosphere reflectance spectra (even if the radiance spectra would happen to be identical). Because the DOAS spectral fit is very sensitive to such jumps from one viewing angle to the other, we observe spurious jumps in the NO_2 columns, with columns retrieved at some of the 60 viewing angles persistently higher or lower than the values at adjacent viewing angles. In priciple, this situation is not different for scanning spectrometers that also contend with irradiance measurement noise and wavelength calibration errors, but since these instruments only have one single detector compared to OMI's 60 viewing angle specific CCD-detectors, such errors do not appear as stripes, but rather as constant, unknown offsets. This means that striping is inherent to hyperspectral imagers with 2-D detectors. Taken together, the jumps in NO_2 columns retrieved from OMI resemble a stripe-like pattern that does not represent "true" geophysical variability in NO_2.

Over relatively clean regions, away from sources of pollution and at low and mid-latitudes, NO_2 columns are not expected to vary significantly across-track. The difference in local time between the far left (west) and far right (east) side of the OMI track is on the order of an hour (depending on latitude), too small to result in an appreciable chemistry-induced decrease between the left (early) and right (later) parts of the orbit (see e.g. Boersma et al., 2008b and Dirksen et al., 2011). We propose here to use a simple box-car averaging method to obtain a better, destriped measure of the true NO_2 column than the original value. For OMI observations between 50° S and the equator, we average total NO_2 columns from 15 adjacent viewing angles for every along-track array of the 60 viewing angles. Because there is no decisive a priori information guiding us to prefer particular viewing angles over others, columns retrieved for different

AMTD
4, 2329–2388, 2011

viewing angles are attributed the same weight. Any 60-element array with more than 17.5% variability is discarded so as to avoid interpreting real geophysical variability (for instance from biomass burning) as spurious across-track variability. We then calculate the average difference between the smoothed and original NO_2 columns between 50° S and the equator as a function of across-track position, map these back to slant column corrections, and subsequently store these as de-striping correction along the complete orbit on a daily basis.

Figure 8 shows corrections for across-track variability computed for three different days in January 2005. Although these corrections have been computed from independent data, they are very similar, reflecting the systematic character of the striping error. The corrections in Fig. 8 are well within 1×10^{15} molec cm^{-2}, a factor 3 smaller than our earlier corrections for retrievals based on Collection 2 data (Boersma et al., 2007). That de-striping corrections for Collection 3 (improved irradiance spectrum calibration) are much smaller than corrections for Collection 2 confirms that the stripes are dominated by across-track jumps in the solar reference spectrum. This is further supported by corrections for July 2005 being highly consistent with those for January 2005. Corrections for later months increase steadily but slowly (not shown), and probably indicate that the 2005 average irradiance measurements are less appropriate as reference spectra for later years. Since 25 June 2007, a number of so-called row anomalies have occurred. These anomalies have affected the quality of level 1B and level 2 data products for particular viewing angles (rows). We have yet to investigate the effectiveness of our destriping method for dates later than 25 June 2007, when a significant number of rows can no longer be used in the boxcar averaging (see also http://www.knmi.nl/omi/research/product/index.php#row).

Figure 9 illustrates the effect of de-striping on monthly mean OMI tropospheric NO_2 columns over Europe in July 2005. We see that the de-striping corrections largely remove the artificial across-track pattern in v1.02. The lower panel of Fig. 9 shows that the local effects of de-striping on the tropospheric columns are strongest over the polluted region of northwestern Europe (up to 0.5×10^{15} molec cm^{-2}), because of the

AMTD
4, 2329–2388, 2011

amplifying effect of low AMF values there (see Fig. 1). Averaged over the large regions of the US, Europe, and China, our destriped NO_2 columns are always within 0.01×10^{15} molec cm^{-2} of the original retrievals (Table 2). We conclude that our destriping has little effect on regional levels of NO_2, but are of importance for local studies, including validation.

5 Impact of the combined algorithm changes

After having discussed individual algorithm improvements, we now combine all the changes to evaluate the overall effect on the DOMINO NO_2 retrievals. Figure 10 and Tables 2 and 3 summarize the impact of the v2.0 algorithm on the DOMINO datasets. The tables illustrate that the sum of the individual changes is not necessarily the same as the overall impact, because some changes counteract others, and because of feedbacks (for instance between albedo and cloud effects, see Boersma et al., 2004). The left panels of Fig. 10 show the absolute differences between DOMINO-derived tropospheric NO_2 columns for the v2.0 and the v1.02 algorithm for January and July 2005. In winter, the changes are strongest (−10% to −20%) over the polluted regions of the world, reflecting the combined effect of individual improvements. The generally reduced NO_2 columns over polluted areas are due to higher AMFs following mainly from our improved altitude-dependent AMFs (look-up table) and also from improved TM4 sampling that results in more NO_2 simulated aloft, where sensitivity to NO_2 is higher. In January 2005, reductions in surface albedo counteract the decreases over the Rhine and Po Valley in Europe, near the Great Lakes in North America, and in interior China. The strong increases in tropospheric NO_2 over these regions result from the lower albedo in the Kleipool et al. (2008) dataset compared to the TOMS/GOME set that suffered from residual snow/ice over these areas (see upper panels of Fig. 4). The right panels in Fig. 10 show the differences between monthly mean v2.0 and v1.02 as a function of the original v1.02 retrieval. The slope of the black triangles in the right

AMTD
4, 2329–2388, 2011

panels of Fig. 10 is somewhat larger in January than in 2005, in line with somewhat stronger relative differences between v2.0 and v1.02 in wintertime.

Summertime changes in retrieved NO_2 (−10%) are smaller than in winter because improved altitude-dependent AMFs for the lowest atmospheric layers have less effect in summer, with relatively more NO_2 aloft, than in winter. Together with the improved sampling of a priori NO_2 profiles from TM4, the improved altitude-dependent AMFs are driving the reductions in tropospheric NO_2, but albedo reductions (Fig. 4) over the UK, parts of China and South Korea lead to the small increases in NO_2 over those areas that can be seen in lower left panel of Fig. 10.

The changes between v1.02 and v2.0 mostly – but not exclusively – reflect the impact of the improved forward model parameters on the retrieval. The changes in the forward model parameters also propagate through the observation operator (averaging kernel) in the data assimilation used to calculate the stratospheric columns (see Boersma et al., 2007; Dirksen et al., 2011). This effect is generally small, as indicated by tropospheric NO_2 columns differences on the order of 10^{13} molec cm^{-2} over the Pacific in Table 2, with the exception of the northern Pacific and the northwestern US (January 2005) where tropospheric NO_2 columns have increased because of reduced stratospheric NO_2 in v2.0. Users of the DOMINO data who apply the averaging kernel can expect the impact of the v2.0 algorithm to be somewhat smaller than indicated in Tables 2 and 3. When using the averaging kernel, the changes in a priori NO_2 profile shape are no longer relevant, and the reductions in NO_2 columns going from v1.02 to v2.0 will be smaller by a few percent.

6 Implicit aerosol correction in DOMINO v2.0

Scattering and absorption by aerosols influence the top-of-atmosphere radiances measured by satellite instruments and can have significant effects on retrievals of atmospheric trace gases and clouds. The sensitivity of the satellite measurements for a particular trace gas can be increased (albedo effect) or decreased (screening), depending

AMTD
4, 2329–2388, 2011

on the amount and optical properties of the aerosols, and its vertical distribution relative to that of the trace gas (e.g. Palmer et al., 2001; Martin et al., 2003; Fu et al., 2007; Leitão et al., 2010). In an earlier study with radiative transfer simulations (Boersma et al., 2004), we found that cloud retrievals are also sensitive to aerosols: higher cloud fractions and lower cloud pressure levels are retrieved in the presence of aerosols compared to a pure molecular scattering atmosphere. The good agreement between explicit corrections for aerosols and the actual correction through the AMF formalism (see Eq. 2) in that study, showed that an implicit correction for aerosols occurs partially through the modified cloud fraction and pressure, at least in theory.

Here we investigate the impact of aerosols on OMI O_2-O_2 and NO_2 retrievals by taking advantage of near-simultaneous satellite measurements of aerosols and clouds from the A-Train (Stephens et al., 2002). We focus on clear-sky situations. MODIS onboard EOS-Aqua observes the Earth's atmosphere approximately 15 min prior to OMI onboard EOS-Aura. We use MODIS-Aqua aerosol optical thickness (AOT) data (Remer et al., 2008) that is retrieved exclusively for cloud-free situations. We subsequently correlate the MODIS observations to any collocated OMI O_2-O_2 cloud parameters whenever the MODIS and OMI measurements were taken within 15 min of another, and store the observations onto a common $0.25^\circ \times 0.25^\circ$ grid. Selecting OMI retrievals that are collocated in space and time with available MODIS AOT retrievals implies that the OMI measurements have been taken under (nearly) cloud-free conditions. In such situations, retrievals of non-zero O_2-O_2 cloud fractions are thus due to aerosol scattering leading to increased top-of-atmosphere radiances. This is in line with the use of a Lambertian reflector with fixed albedo (0.8) as the simplified model in the O_2-O_2 retrieval. The fractional coverage of the Lambertian reflector that yields a top-of-atmosphere reflectance that best agrees with the observed reflectance, is interpreted as the radiometrically equivalent, or effective, cloud fraction (Stammes et al., 2008). The O_2-O_2 retrieval does not distinguish between clouds or aerosols to explain the observed reflectances.

AMTD
4, 2329–2388, 2011

The upper panel of Fig. 11 shows the monthly mean AOT from MODIS-Aqua (470 nm) for July 2005 over the eastern US. The middle panel shows the corresponding monthly mean of O_2-O_2 effective cloud fractions from OMI sampled at the same locations and same time as the MODIS observations. We see that the AOT values are highest (up to 0.7) over the southeastern US, and that this is reflected by effective cloud fractions with values up to 0.15. The MODIS Ångström exponent over the eastern US is approximately 1.75, corresponding to small particles (e.g. Dubovik et al., 2002; Russell et al., 2010). Upon inspection of the OMI Absorbing Aerosol Index (Torres et al., 1998) during July 2005, we did not find any evidence for a significant contribution from absorbing particles to the AOT. Instead, there is strong evidence that the high aerosol loadings originate from local emissions of volatile organic compounds (e.g. Goldstein et al., 2009; Jiang et al., 2010; Veefkind et al., 2011), and these aerosols are known to be highly reflective (Penning de Vries et al., 2009). Figure 12 shows significant positive correlation (r=0.66, n=9685) between OMI effective cloud fractions and MODIS AOT over the eastern US. A reduced major axis regression suggests that the OMI effective cloud fractions can be expressed as $f_{cl} = 0.21 \times \tau$, with τ the MODIS AOT. We conclude that OMI cloud retrievals are sensitive to the presence of scattering aerosols, particularly in situations with predominantly scattering aerosols, such as over the southeastern US in July 2005.

The lower panel of Fig. 11 shows the monthly mean O_2-O_2 effective cloud pressures over the eastern US in July 2005. In the absence of enhanced effective cloud fractions, the O_2-O_2 retrieval essentially returns values close to surface pressure (Acarreta et al., 2004) such as for the northern part of the domain. For high AOT (increased effective cloud fractions) in the southeastern US, O_2-O_2 pressures are lowest, indicative of elevated aerosol layers. The median O_2-O_2 pressure corresponds to 720 hPa for hazy situations with MODIS AOT > 0.2. This is consistent with significant amounts of aerosols well above the boundary layer in the summertime (south)eastern US as observed with ground-based, airborne, and space-based lidars (Turner et al., 2001; Liu et al., 2008; Lewis et al., 2010). We examine the vertical differences between the cloud

AMTD
4, 2329–2388, 2011

pressures and the a priori NO_2 profile, by comparing the probability distribution of cloud pressures to the average NO_2 vertical distribution simulated by TM4 under "hazy" conditions (AOT > 0.2). Figure 13 (lower panel) shows that the scattering levels (due to aerosol scattering) mostly reside above the bulk of the NO_2 in July 2005. A layer of scattering aerosols well above an NO_2 layer is most likely to have a screening effect, i.e. reduce the AMF compared to situations without aerosols. This is not different from the effect of clouds above a polluted layer that also tend to decrease the AMF (see for example Fig. 5a–b in Boersma et al., 2004).

We investigate whether an implicit AMF aerosol correction occurs through Eq. (2) with modified cloud parameters, now that we have shown that OMI cloud retrievals are obviously sensitive to scattering aerosols. Figure 14 shows the ratio of OMI NO_2 AMFs calculated in our standard retrieval with the small, positive effective cloud fractions resulting from aerosol scattering (M) to the clear-sky AMFs (M_{cr}) with zero cloud fraction (consistent with successful MODIS AOT retrievals in the absence of clouds). This implicit aerosol correction factor, defined as M/M_{cr}, is 0.8–1.0 in the "hazy" region where AOT > 0.2, and close to 1.0 in the northern part of the domain with low AOT and small cloud fractions. Indeed, AMFs influenced by aerosols through the modified O_2-O_2 cloud parameters are smaller than clear-sky AMFs, consistent with the expected screening effect. To evaluate our implicit corrections, we also calculated correction factors from simulations with a separate, independent radiative transfer model (SCIATRAN 2.2, Rozanov et al., 2005). SCIATRAN AMFs were calculated at 440 nm for a summertime southern US scenario with the average "hazy" TM4 NO_2 profile shown in Fig. 13, with and without aerosols. For the simulations with aerosols, we used an AOT (440 nm) of 0.5, in line with the MODIS observations in Fig. 11. We used aerosol profiles with significant extinction up to 3–4 km (box profile, and profiles observed by CALIOP and simulated by GOCART over the eastern US from Yu et al., 2010), in line with the OMI O_2-O_2 pressure levels around 700 hPa (Fig. 13). We assumed a surface albedo of 0.05 (0.054 for summer, 0.049 for winter), consistent with the Kleipool et al. (2008) albedo climatology, and the aerosols to consist mostly of small particles

AMTD
4, 2329–2388, 2011

with phase functions consistent with long-term AERONET observations summarized by Dubovik et al. (2002) (single scattering albedo 0.97 in summer, 0.95 in winter). Table 5 shows that the SCIATRAN simulations result in aerosol correction factors of 0.97–1.11, which is higher than our satellite-inferred implicit correction factors. The SCIATRAN simulations that agree most with our implicit correction factors, with values < 1.0, are the ones with the average "hazy" TM4 NO_2 profile (Fig. 13) replaced by a 1 km NO_2 "box profile". Apparently, for screening by a haze layer to occur, most of the NO_2 needs to be well below the bulk of the aerosol particles. We conclude that our satellite-inferred implicit correction factors are 10–20% lower than the explicit correction factors simulated with the SCIATRAN radiative transfer model. To investigate whether this discrepancy reflects a systematic error in our approach, or inadequate assumptions on aerosol and NO_2 characteristics used in the SCIATRAN simulations, we recommend to repeat this type of analysis for situations where most of the aerosol and NO_2 characteristics are known, such as during dedicated measurement campaigns such as DANDELIONS (Hains et al., 2010) or CINDI (Piters et al., 2011).

Compared to summertime retrievals, the impact of aerosols on wintertime retrievals is modest. Figure 15 shows monthly mean MODIS AOT values for January 2005 up to 0.3, much smaller than in summer. The MODIS Ångström exponent over areas with high AOT is 0.7, indicating that particles are coarser in winter than in summer and that these coarse particles dominate over the ocean (Dubovik et al., 2002). Previous studies showed that lower AOT and coarse particles affect AMFs less than high AOT and fine particles (Boersma et al., 2004; Leitão et al., 2010). Figure 15 also shows that both AOT values and cloud fractions are enhanced over the western Atlantic, and both are low over the southern US. There is positive correlation between AOT and cloud fractions over the domain ($r = 0.42$, $n = 4465$) in January, but it is less significant than in July 2005. The lower panel of Fig. 15 shows that aerosol-induced cloud pressures are high in January compared to July 2005, indicating that the scattering aerosols reside closer to the surface in winter. Indeed, the median O_2-O_2 pressure corresponds to 830 hPa when MODIS AOT > 0.1. Figure 13 indicates that in winter, aerosols are more

AMTD
4, 2329–2388, 2011

likely to be mixed with NO_2 than in summer, but also that aerosols can still be elevated relative to the NO_2 layer. We can thus expect AMFs to be enhanced in some circumstances (when the aerosols are mixed with the NO_2 layer) and reduced in others (when aerosols are well above the NO_2 layer, as in summer). Indeed, Fig. 14 (upper panel) shows most (implicit) aerosol correction factors in the range 0.9–1.1. SCIATRAN correction factors for a number of plausible wintertime scenarios with and without aerosols over the eastern US are similar with values in the 0.95–1.10 range. Table 6 confirms that correction factors are lowest for the scenario with the most elevated aerosol (2 km box profile).

7 Conclusions

We have improved the Dutch OMI NO_2 (DOMINO) algorithm for global retrievals of tropospheric NO_2 columns from the Ozone Monitoring Instrument. DOMINO was first described in Boersma et al. (2007), and has been used sucessfully in many scientific applications since then. Various validation exercises suggest that the previous version (v1.02) of DOMINO retrievals was of good quality, but biased high by 0–40%, mostly because of air mass factor errors.

Here we focused especially on improving the NO_2 air mass factors in order to generate a new DOMINO tropospheric NO_2 dataset, named version 2 (v2.0). The improvements concern a better description of the radiative transfer for the lowest atmospheric layers, surface albedo, terrain height, clouds, and a priori vertical NO_2 profiles. We have calculated a new altitude-dependent air mass factor look-up table (LUT) based on a more realistic atmospheric profile, and with an increased number of reference vertical layers and surface albedos, which reduces interpolation errors. The new LUT also mends another interpolation error in the computation of the altitude-dependent air mass factors for the lowest atmospheric layer. We showed that the new LUT alone increases air mass factors by 20–30%, thereby reducing retrieved columns by up to 20%.

AMTD
4, 2329–2388, 2011

We implemented a recently developed surface albedo climatology based on measurements from OMI in both the NO_2 and cloud retrieval. The OMI surface albedo database with improved spatial resolution ($0.5^\circ \times 0.5^\circ$) reduces cloud and snow/ice contamination in the surface albedo, and leads to lower cloud fractions compared to TOMS/GOME. The overall impact of the OMI albedo is generally modest in summer but can be strong (up to +10%) in winter over polluted regions that previously suffered from residual snow or ice in the TOMS/GOME database. We improved the sampling of the TM4 model, resulting in a priori NO_2 profiles that are better mixed throughout the boundary layer. The TM4 profiles were also compared with in situ measurements from the INTEX-A/ICARTT and INTEX-B aircraft campaigns, showing good consistency throughout the lower troposphere. The improved sampling of NO_2 from TM4 leads to more NO_2 aloft and higher air mass factors over polluted regions. The strongest impact on NO_2 retrievals is in summer (up to −8%), when vertical transport is stronger than in winter. We reduced topography-related errors by replacing the $2^\circ \times 3^\circ$ TM4 surface pressures by more accurate values based on the high-resolution DEM_3km database, and scaling the a priori TM4 NO_2 accordingly. We found small changes (<1%) in tropospheric NO_2 columns over extended polluted regions, but significant enhancements (up to 14%) in winter over polluted areas that previously had too high terrain heights such as the Po Valley and Beijing, and we found similar decreases for polluted highlands such as Mexico City and the Highveld area in South Africa that had too low terrain heights.

Apart from the air mass factor improvements, we introduced an a posteriori correction for stripes that are still apparent in the v1.02 tropospheric NO_2 columns based on Collection 3 level 1 data. Our correction is based on the assumption that the jumps in NO_2 slant columns that occur from one OMI viewing angle to the other are unrealistic, and that a simple per-orbit low-pass filter effectively eliminates them. Averaged over polluted areas, the effect of the stripe correction is marginal (<1%), but locally the correction of tropospheric NO_2 columns is on the order of 0.5×10^{15} molec cm^{-2}.

AMTD
4, 2329–2388, 2011

The picture that emerges from the individual improvements is that our new LUT and the improved sampling of TM4 have a significant effect on the NO_2 retrievals for the polluted regions in the world. For users taking the averaging kernel into account – such as data assimilation groups – the improved TM4 sampling of NO_2 is not relevant, and the changes between v1.02 and v2.0 will be somewhat smaller. The overall impact of the OMI surface albedo dataset, the improved description of the terrain height, and the stripe correction, is modest on average (changes are typically a few percent) over large polluted areas, but still causes significant changes on the local scale. These improvements are important, since our satellite measurements are often used for studies with a distinct regional (air quality) or even local character (trend and validation studies).

Our new DOMINO v2.0 retrievals of tropospheric NO_2 columns are reduced by 20% in winter, and by 10% during summer compared to v1.02 over extended polluted regions. These reductions are mainly driven by the improved air mass factor look-up table, and the better sampling of a priori NO_2 profiles from TM4. On smaller spatial scales, the differences between v2.0 and v1.02 can be larger, reflecting the sometimes considerable changes in local surface albedo, clouds, and terrain height, and the effects of destriping. These reductions would bring DOMINO tropospheric columns in better agreement with independent measurements and model simulations. The conclusions of most published studies based on previous DOMINO v1.02 retrievals remain intact when they would be repeated with the improved v2.0 set, often because those studies made use of the averaging kernels, or because they were mainly concerned with relative changes in the NO_2 data. Absolute values for NO_x emissions directly estimated from our previous DOMINO retrievals (e.g. Boersma et al., 2008b; Zhao and Wang, 2009) were probably too high by 10–20%, but generally still well within the stated limits of uncertainty.

Following up on our earlier work that predicted OMI cloud retrievals to be sensitive to the presence of scattering aerosols, we examined the relationship between concurrent OMI O_2-O_2 cloud observations and MODIS-Aqua aerosol optical thickness (AOT) over the eastern US. We found that high aerosol loadings tend to increase retrieved O_2-O_2

AMTD
4, 2329–2388, 2011

effective cloud fractions with reduced cloud pressures, especially over the southeastern US which is covered by a layer of elevated, small (scattering) particles during Summer. The combined effect of the enhanced summertime cloud parameters on the NO_2 retrieval corresponds to screening: OMI has become less sensitive to NO_2 because of the elevated aerosol layer residing above the NO_2 layer. In the DOMINO retrieval, the aerosol correction proceeds implicitly through the air mass factor formulation. The aerosol-induced cloud parameters reduce air mass factors over the southeastern US by up to 20% in summertime. In winter, aerosol loadings are lower, particles are coarser, and air mass factors are much less affected. Radiative transfer calculations with crudely estimated aerosol and NO_2 parameters reproduced the range of implicit aerosol correction factors for the winter case, but were higher by 0–20% in summer. Radiative transfer calculations with observed rather than guessed NO_2 and aerosol parameters are required to further investigate this discrepancy, and provide more insight into the exact influence that aerosols exert on cloud and trace gas retrievals.

We focused here on NO_2 retrievals from OMI, but the described improvements are of similar importance for NO_2 retrievals from the GOME, SCIAMACHY, and GOME-2 series provided by KNMI on www.temis.nl. The new altitude-dependent air mass factor look-up table, a more realistic surface albedo dataset (from MERIS, see Popp et al., 2011), the improved description of terrain height, and better sampling of TM4 profiles are currently being implemented in the GOME(-2) and SCIAMACHY NO_2 retrievals and preliminary results indicate similar effects on those retrievals as found here for OMI. New versions of the GOME(-2) and SCIAMACHY NO_2 data products can be expected in 2011. The new v2.0 DOMINO NO_2 retrievals are currently being made available (data for 2004–2007 is already online) on www.temis.nl.

AMTD
4, 2329–2388, 2011

Acknowledgements. We wish to thank Randall Martin (Dalhousie University) for encouraging discussions. NO_2 measurements from the NASA DC-8 aicraft were made available by R. C. Cohen and co-workers (University of California, Berkeley), and from the NOAA's WP-3D aircraft by Tom Ryerson (NOAA). We acknowledge the free use of MODIS Aqua aerosol optical thickness data, obtained from http://ladsweb.nascom.nasa.gov, and publicly available information derived from the AERONET database. This work was supported by a Vidi grant (864.09.001) by the Netherlands Organisation for Scientific Research (NWO).

References

Acarreta, J. R., de Haan, J. F., and Stammes, P.: Cloud pressure retrieval using the O_2-O_2 absorption band at 477 nm, J. Geophys. Res., 109, D05204, doi:10.1029/2003JD003915, 2004. 2337, 2338, 2343, 2353

Basset, M. and Seinfeld, J. H.: Atmospheric Equilibrium Model of Sulfate and Nitrate Aerosols, Atmos. Environ., 17(11), 2237–2252, 1983. 2331

Blond, N., Boersma, K. F., Eskes, H. J., van der A, R. J., Van Roozendael, M., De Smedt, I., Bergamatti, G., and Vautard, R.: Intercomparison of SCIAMACHY nitrogen dioxide observations, in situ measurements and air quality modeling results over Western Europe, J. Geophys. Res., 112, D10311, doi:10.1029/2006JD007277, 2007.

Boersma, K. F., Bucsela, E. J., Brinksma, E. J., and Gleason, J. F.: NO_2, in: OMI Algorithm Theoretical Basis Document, vol. 4, OMI Trace Gas Algorithms, ATB-OMI-04, Version 2.0, edited by: Chance, K., NASA Distrib. Active Archive Cent., Greenbelt, Md., 13-36, 2002. 2335, 2337

Boersma, K. F., Eskes, H. J., and Brinksma, E. J.: Error analysis for tropospheric NO_2 retrieval from space, J. Geophys. Res., 109, D04311, doi:10.1029/2003JD003962, 2004. 2332, 2333, 2336, 2337, 2344, 2347, 2350, 2352, 2354, 2355

Boersma, K. F., Eskes, H. J., Veefkind, J. P., Brinksma, E. J., van der A, R. J., Sneep, M., van den Oord, G. H. J., Levelt, P. F., Stammes, P., Gleason, J. F., and Bucsela, E. J.: Near-real time retrieval of tropospheric NO_2 from OMI, Atmos. Chem. Phys., 7, 2103–2118, doi:10.5194/acp-7-2103-2007, 2007. 2332, 2335, 2349, 2351, 2356

Boersma, K. F., Jacob, D. J., Eskes, H. J., Pinder, R. W., and Wang, J.: Intercomparison of SCIAMACHY and OMI tropospheric NO_2 columns: Observing the diurnal evolution of chemistry and emissions from space, J. Geophys. Res., 113, D16S26, doi:10.1029/2007JD008816, 2008a. 2332, 2346

Boersma, K. F., Jacob, D. J., Bucsela, E. J., Perring, A. E., Dirksen, R., van der A, R. J., Yantosca, R. M., Park, R. J., Wenig, M. O., Bertram, T. H., and Cohen, R. C.: Validation of OMI tropospheric NO_2 observations during INTEX-B and application to constrain NO_x emissions over the eastern United States and Mexico, Atmos. Environ., 42(19), 4480–4497, doi:10.1016/j.atmosenv.2008.02.004, 2008b. 2348, 2358

Boersma, K. F., Jacob, D. J., Trainic, M., Rudich, Y., DeSmedt, I., Dirksen, R., and Eskes, H. J.: Validation of urban NO_2 concentrations and their diurnal and seasonal variations observed from the SCIAMACHY and OMI sensors using in situ surface measurements in Israeli cities, Atmos. Chem. Phys., 9, 3867–3879, doi:10.5194/acp-9-3867-2009, 2009a. 2332

Boersma, K. F., Dirksen, R. J., Veefkind, J. P., Eskes, H. J., and Van der A, R. J.: Dutch OMI NO_2 (DOMINO) data product HE5 data file user manual, TEMIS website, http://www.temis.nl/airpollution/no2.html (last access: April 2011), 2009b. 2332, 2335

Bovensmann, H., Burrows, J. P., Buchwitz, M., Frerick, J., Noel, S., Chance, K. V., and Goede, A. P. H.: SCIAMACHY: Mission objectives and measurement modes, J. Atmos. Sci., 56(2), 127–150, 1999. 2331

Bucsela, E. J., Celarier, E. A., Wenig, M. O., Gleason, J. F., Veefkind, J. P., Boersma, K. F., and Brinksma, E. J.: Algorithm for NO_2 vertical column retrieval from the Ozone Monitoring Instrument, IEEE T. Geosci. Remote, 44(5), 1245–1258, doi:10.1109/TGRS.2005.863715, 2006. 2332, 2335

Burrows, J. P., Weber, M., Buchwitz, M., Rozanov, V. V., Ladstatter-Weissenmayer, A., Richter, A., DeBeek, R., Hoogen, R., Bramstedt, K., and Eichmann, K. U.: The Global Ozone Monitoring Experiment (GOME): Mission concept and first scientific results, J. Atmos. Sci., 56, 151–175, 1999. 2331

Callies, J., Corpaccioli, E., Eisinger, M., Hahne, A., and Lefebvre, A.: GOME-2 – Metop's Second-Generation Sensor for Operational Ozone Monitoring, ESA Bull., 102, 28–36, 2000. 2332

de Haan, J. F., Bosma, P. B., and Hovenier, J. W.: The adding method for multiple scattering calculations of polarized light, Astron. Astrophys., 183, 371-393, 1987.

AMTD
4, 2329–2388, 2011

Dentener, F., van Weele, M., Krol, M., Houweling, S., and van Velthoven, P.: Trends and inter-annual variability of methane emissions derived from 1979–1993 global CTM simulations, Atmos. Chem. Phys., 3, 73–88, doi:10.5194/acp-3-73-2003, 2003. 2335

Dirksen, R. J., Boersma, K. F., Eskes, H. J., Ionov, D. V., Bucsela, E. J., Levelt, P. F., and Kelder, H. M.: Evaluation of stratospheric NO_2 retrieved from the Ozone Monitoring Instrument: Intercomparison, diurnal cycle, and trending, J. Geophys. Res., 116, D08305, doi:10.1029/2010JD014943, 2011. 2333, 2335, 2348, 2351

Dobber, M. R., Dirksen, R., Levelt, P., van den Oord, G. H. J., Voors, R., Kleipool, Q., Jaross, G., Kowalewski, M., Hilsenrath, E., Leppelmeier, G., de Vries, J., Dierssen, W., and Rozemeijer, N.: Ozone Monitoring Instrument calibration, IEEE T. Geosci. Remote, 44, 1209-1238, 2006.

Dobber, M., Kleipool, Q., Dirksen, R., Levelt, P. F., Jaross, G., Taylor, S., Kelly, T., Flynn, L., Leppelmeier, G., and Rozemeijer, N.: Validation of Ozone Monitoring Instrument level 1b data products, J. Geophys. Res., 113, D15S06, doi:10.1029/2007JD008665, 2008. 2334

Dubovik, M., Holben, B., Eck, T. F., Smirnov, A., Kaufman, Y. J., King, M. D., Tanré, D., and Slutsker, I.: Variability of absorption and Optical Properties of Keu Aerosol Types Observed in Worldwide Locations, J. Atmos. Sci., 59, 590–608, 2002. 2353, 2355

Eskes, H. J. and Boersma, K. F.: Averaging kernels for DOAS total-column satellite retrievals, Atmos. Chem. Phys., 3, 1285–1291, doi:10.5194/acp-3-1285-2003, 2003. 2336, 2337, 2347

Fu, T.-M., Jacob, D. J., Palmer, P. I., Chance, K., Wang, Y. X., Barletta, B., Blake, D. R., Stanton, J. C., and Pilling, M. J.: Space-based formaldehyde measurements as constraints on volatile organic compound emissions in east and south Asia and implications for ozone, J. Geophys. Res., 112, D06312, doi:10.1029/2006JD007853, 2007. 2352

Goldstein, A., Koven, C. D., Heald, C. L., and Fung, I. Y.: Biogenic carbon and anthropogenic pollutants combine to form a cooling haze over the southeastern United States, P. Natl. Acad. Sci., 106(22), 8835–8840, doi:10.1073/pnas.0904128106, 2009. 2353

Hains, J. C., Boersma, K. F., Kroon, M., Dirksen, R. J., Cohen, R. C., Perring, A. E., Bucsela, E. J., Volten, H., Swart, D. P. J., Richter, A., Wittrock, F., Schoenhardt, A., Wagner, T., Ibrahim, O. W., Van Roozendael, M., Pinardi, G., Gleason, J. F., Veefkind, J. P., and Levelt, P. F.: Testing and improving OMI DOMINO tropospheric NO_2 using observations from the DANDELIONS and INTEX-B validation campaigns, J. Geophys. Res., 115, D05301, doi:10.1029/2009JD0012399, 2010. 2344, 2346, 2355

Holland, E. A. and Lamarque, J.-F.: Modelling bio-atmospheric coupling of the nitrogen cycle through NO_x emissions and NO_y deposition, Nutr. Cycl. Agroecosyst., 48, 7–24, 1997. 2331

AMTD
4, 2329–2388, 2011

Holtslag, A. A. and Boville, B. A.: Local versus nonlocal boundary layer diffusion in a global climate model, J. Climate, 10, 1825–1842, 1993. 2346

Huijnen, V., Eskes, H. J., Poupkou, A., Elbern, H., Boersma, K. F., Foret, G., Sofiev, M., Valdebenito, A., Flemming, J., Stein, O., Gross, A., Robertson, L., D'Isidoro, M., Kioutsioukis, I., Friese, E., Amstrup, B., Bergstrom, R., Strunk, A., Vira, J., Zyryanov, D., Maurizi, A., Melas, D., Peuch, V.-H., and Zerefos, C.: Comparison of OMI NO_2 tropospheric columns with an ensemble of global and European regional air quality models, Atmos. Chem. Phys., 10, 3273–3296, doi:10.5194/acp-10-3273-2010, 2010. 2333, 2344

Jacob, D. J., Heikes, E. G., Fan, S.-M., Logan, J. A., Mauzerall, D. L., Bradshaw, J. D., Singh, H. B., Gregory, G. L., Talbot, R. W., Blake, D. R., and Sachse, G. W.: Origin of ozone and NO_x in the tropical troposphere: A photochemical analysis of aircraft observations over the South Atlantic basin, J. Geophys. Res., 101, 24235–24250, 1996. 2331

Jiang, X., Yang, Z.-L., Liao, H., and Wiedinmyer, C.: Sensitivity of biogenic secondary organic aerosols to future climate change at regional scales: an online coupled simulation, Atmos. Environ., 44, 4891–4907, 2010. 2353

Kleipool, Q. L., Dobber, M. R., de Haan, J. F., and Levelt, P. F.: Earth surface reflectance climatology from 3 years of OMI data, J. Geophys. Res., 113, D18308, doi:10.1029/2008JD010290, 2008. 2336, 2337, 2338, 2341, 2343, 2350, 2354

Koelemeijer, R. B. A., Stammes, P., Hovenier, J. W., and de Haan, J. F.: A fast method for retrieval of cloud parameters using oxygen A band measurements from the Global Ozone Monitoring Experiment, J. Geophys. Res., 106, 3475-3490, doi:10.1029/2000JD900657, 2001. 2342

Koelemeijer, R. B. A., de Haan, J. F., and Stammes, P.: A database of spectral surface reflectivity in the range 335-772 nm derived from 5.5 years of GOME observations, J. Geophys. Res., 108(D2), 4070, doi:10.1029/2002JD002429, 2003.

Lamsal, L. N., Martin, R. V., van Donkelaar, A., Celarier, E. A., Bucsela, E. J., Boersma, K. F., Dirksen, R., Luo, C., and Wang, Y.: Indirect validation of tropospheric nitrogen dioxide retrieved from the Ozone Monitoring Instrument: Insight into the seasonal variation of nitrogen oxides at northern midlatitudes, J. Geophys. Res., 115, D05301, doi:10.1029/2009JD012399, 2010. 2333

Leitão, J., Richter, A., Vrekoussis, M., Kokhanovsky, A., Zhang, Q. J., Beekmann, M., and Burrows, J. P.: On the improvement of NO_2 satellite retrievals - aerosol impact on the airmass factors, Atmos. Meas. Tech., 3, 475–493, doi:10.5194/amt-3-475-2010, 2010. 2352, 2355

AMTD
4, 2329–2388, 2011

Leue, C., Wenig, M., Wagner, T., Klimm, O., Platt, U., and Jähne, B.: Wuantitative analysis of NO_x emissions from Global Ozone Monitoring Experiment satellite image sequences, J. Geophys. Res., 106, 5493–5505, doi:10.1029/2000JD900572, 2001. 2331

Levelt, P. F., van den Oord, G. H. J., Dobber, M. R., Malkki, A., Visser, H., de Vries, J., Stammes, P., Lundell, J., and Saari, H.: The Ozone Monitoring Instrument, IEEE T. Geosci. Remote, 44, 1093–1101, 2006. 2331

Lewis, J., De Young, R., and Chu, D. A.: A Study of Air Quality in the Southeastern Hampton-Norfolk-Virginia Beach Region with Airborne Lidar Measurements and MODIS Aerosol Optical Depth Retrievals, J. Appl. Meteorol. Clim., 49, 3–19, doi:10.1175/2009JAMC2119.1, 2010. 2353

Lin, J.-T. and McElroy, M.: Impacts of boundary layer mixing on pollutant vertical profiles in the lower troposphere: Implications to satellite remote sensing, Atmos. Environ., 44(14), 1726–1739, doi:10.1016/j.atmosenv.2010.02.009, 2010. 2346

Liu, D., Wang, Z., Liu, Z., Winker, D., and Trepte, C.: A height resolved global view of dust aerosols from the first year CALIPSO lidar measurements, J. Geophys. Res., 113, D16214, doi:10.1029/2007JD009776, 2008. 2353

Martin, R. V., Jacob, D. J., Chance, K., Kurosu, T. P., Palmer, P. I., and Evans, M. J.: An improved retrieval of tropospheric nitrogen dioxide from GOME, J. Geophys. Res., 107(D20), 4437, doi:10.1029/2001JD001027, 2002. 2331, 2337

Martin, R. V., Jacob, D. J., Chance, K., Kurosu, T. P., Palmer, P. I., and Evans, M. J.: Global inventory of nitrogen oxide emissions constrained by space-based observations, J. Geophys. Res., 108(D17), 4537, doi:10.1029/2003JD003453, 2003. 2352

Martin, R. V., Sioris, C. E., Chance, K., Ryerson, T. B., Bertram, T. H., Wooldridge, P. J., Cohen, R. C., Neuman, J. A., Swanson, A., and Flocke, F. M.: Evaluation of space-based constraints on global nitrogen oxide emissions with regional aircraft measurements over and downwind of eastern North America, J. Geophys. Res., 111, D15308, doi:10.1029/2005JD006680, 2006. 2346

Michaels, A. F., Olson, D., Sarmiento, J. L., Ammerman, J. W., Fanning, K., Jahnke, R., Knap, A. H., Lipschultz, F., and Prospero, J. M.: Inputs, losses, and transformations of nitrogen and phosphorus in the pelagic North Atlantic Ocean, Biogeochemistry, 35, 181–226, 1996. 2331

Palmer, P. I., Jacob, D. J., Chance, K., Martin, R. V., Spurr, R. J. D., Kurosu, T. P., Bey, I., Yantosca, R., Fiore, A., and Li, Q.: Air mass factor formulation for spectroscopic measurements from satellites: Application to formaldehyde retrievals from the Global Ozone Monitoring

Experiment, J. Geophys. Res., 106, 14539-14550, 2001. 2336, 2352
Penning de Vries, M. J. M., Beirle, S., and Wagner, T.: UV Aerosol Indices from SCIAMACHY: introducing the SCattering Index (SCI), Atmos. Chem. Phys., 9, 9555–9567, doi:10.5194/acp-9-9555-2009, 2009. 2353
Piters, A., Boersma, K. F., Kroon, M., Hains, J. C., Van Roozendael, M., Wittrock, F., Roscoe, H., du Piesanie, A., and Klein-Baltink, H.: The Cabauw Intercomparison campaign for Nitrogen Dioxide Measuring Instruments (CINDI): Design, execution, and first results, to be submitted to Atmos. Meas. Tech. Discuss., 2011. 2355
Popp, C., Wang, P., Brunner, D., Stammes, P., Zhou, Y., and Grzegorski, M.: MERIS albedo climatology for FRESCO+ O_2 A-band cloud retrieval, Atmos. Meas. Tech., 4, 463–483, doi:10.5194/amt-4-463-2011, 2011. 2359
Remer, L. A., Kleidman, R. G., Levy, R. C., Kaufman, Y. J., Tanre, D., Mattoo, S., Vanderlei Martins, J., Ichoku, C., Koren, I., Yu, H., and Holben, B. N.: Global aerosol climatology from the MODIS satellite sensors, J. Geophys. Res., 113, D14S07, doi:10.1029/2007JD009661, 2008. 2352
Richter, A., Burrows, J. P., Nüss, H., Granier, C., and Niemeier, U.: Increase in tropospheric nitrogen dioxide over China observed from space, Nature, 437, 129–132, 2005. 2331
Rozanov, A., Rozanov, V., Buchwitz, M., Kokhanovsky, A., and Burrows, J. P.: SCIATRAN 2.0 - A new radiative transfer model for geophysical applications in the 175–2400 nm spectral region, Adv. Space Res., 36(5), 1015–1019, doi:10.1016/j.asr.2005.03.012, 2005. 2354
Russell, P. B., Bergstrom, R. W., Shinozuka, Y., Clarke, A. D., DeCarlo, P. F., Jimenez, J. L., Livingston, J. M., Redemann, J., Dubovik, O., and Strawa, A.: Absorption Angstrom Exponent in AERONET and related data as an indicator of aerosol composition, Atmos. Chem. Phys., 10, 1155–1169, doi:10.5194/acp-10-1155-2010, 2010. 2353
Ryerson, T. B., Williams, E. J., and Fehsenfeld, F. C.: An efficient photolysis system for fast-response NO_2 measurements, J. Geophys. Res., 105(D21), 26447–26461, 2000. 2345
Schaub, D., Brunner, D., Boersma, K. F., Keller, J., Folini, D., Buchmann, B., Berresheim, H., and Staehelin, J.: SCIAMACHY tropospheric NO_2 over Switzerland: estimates of NO_x lifetimes and impact of the complex Alpine topography on the retrieval, Atmos. Chem. Phys., 7, 5971–5987, doi:10.5194/acp-7-5971-2007, 2007.
Shindell, D. T., Faluvegi, G., Koch, D. M., Schmidt, G. A., Unger, N., and Bauer, S. E.: Improved Attribution of Climate Forcing to Emissions, Science, 326, 716–718, doi:10.1126/science.1174760, 2009. 2331

AMTD
4, 2329–2388, 2011

Spichtinger N., Wenig, M., James, P., Wagner, T., Platt, U., and Stohl, A.: Satellite detection of a continental-scale plume of nitrogen oxides from boreal fires, Geophys. Res. Lett., 29, 4579–4583, 2001. 2331

Stammes, P.: Spectral radiance modeling in the UV-visible range, in: IRS200: Current Problems in Atmospheric Radiation, edited by: Smith, W. L. and Timofeyev, Y. M., A. Deepak, Hampton, Va., 385–388, 2001.

Stammes, P., Sneep, M., de Haan, J. F., Veefkind, J. P., Wang, P., and Levelt, P. F.: Effective cloud fractions from the Ozone Monitoring Instrument: Theoretical framework and validation, J. Geophys. Res., 113, D16S38, doi:10.1029/2007JD008820, 2008. 2341, 2352

Stephens, G. L., Vane, D. G., Boain, R. J., Mace, G. G., Sassen, K., Wang, Z., Illingworth, A. J., O'Connor, E. J., Rossow, W. B., Durden, S. L., Miller, S. D., Austin, R. T., Benedetti, A., Mitrescu, C., and the CloudSat Science Team: The CloudSat Mission and the A-Train, B. Am. Meteorol. Soc., 83, 1771–1790, 2002. 2352

Thornton, J. A., Wooldridge, P. J., and Cohen, R. C.: Atmospheric NO_2: In situ laser-induced fluorescence detection at parts per trillion mixing ratios, Anal. Chem., 72, 528–539, 2000. 2345

Torres, O., Bhartia, P. K., Herman, J. R., Ahmad, Z., and Gleason, J.: Derivation of aerosol properties from a satellite measurement of backscattered ultraviolet radiation: Theoretical basis, J. Geophys. Res., 103, 17099–17110, 1998. 2353

Turner, D. D., Ferrare, R. R., and Brasseur, L. A.: Average Aerosol Extinction and Water Vapor Profiles Over the Southern Great Plains, Geophys. Res. Lett., 28(23), 4441–4444, 2001. 2353

van der A, R. J., Eskes, H. J., Boersma, K. F., van Noije, T. P. C., Van Roozendael, M., De Smedt, I., Peters, D. H. M. U., and Meijer, E. W.: Trends, seasonal variability and dominant NO_x source derived from a ten year record of NO_2 measured from space, J. Geophys. Res., 113, D04302, doi:10.1029/2007JD009021, 2008. 2331

Veefkind, J. P., Boersma, K. F., Wang, J., Kurosu, T. P., Krotkov, N., Chance, K., and Levelt, P. F.: Global satellite analysis of the relation between aerosols and short-lived trace gases, Atmos. Chem. Phys., 11, 1255–1267, doi:10.5194/acp-11-1255-2011, 2011. 2353

Wang, Y., McElroy, M. B., Boersma, K. F., Eskes, H. J., and Veefkind, J. P.: Traffic restrictions associated with the Sino-African summit: Reductions of NO_x detected from space, Geophys. Res. Lett., 34, L08814, doi:10.1029/2007GL029326, 2007. 2332

AMTD
4, 2329–2388, 2011

Yu, H., Chin, M., Winker, D. M., Omar, H., Liu, Z., Kittaka, C., and Diehl, T.: Global view of aerosol vertical distributions from CALIPSO lidar measurements and GOCART simulations: Regional and seasonal variations, J. Geophys. Res., 115, D00H30, doi:10.1029/2009JD013364, 2010. 2354, 2372

Zhao, C. and Wang, Y.: Assimilated inversion of NO_x emissions over east Asia using OMI NO_2 column measurements, Geophys. Res. Lett., 36, L06805, doi:10.1029/2008GL037123, 2009. 2358

Zhou, Y., Brunner, D., Boersma, K. F., Dirksen, R., and Wang, P.: An improved tropospheric NO_2 retrieval for OMI observations in the vicinity of mountainous terrain, Atmos. Meas. Tech., 2, 401–416, doi:10.5194/amt-2-401-2009, 2009. 2338, 2339

Zhou, Y., Brunner, D., Spurr, R. J. D., Boersma, K. F., Sneep, M., Popp, C., and Buchmann, B.: Accounting for surface reflectance anisotropy in satellite retrievals of tropospheric NO_2, Atmos. Meas. Tech., 3, 1185–1203, doi:10.5194/amt-3-1185-2010, 2010.

AMTD
4, 2329–2388, 2011

Table 1. Summary of validation studies with DOMINO v1.02 tropospheric NO_2 data.

Study	Region	Period	Independent data	Result	Recommendation
Boersma et al. (2009)	Israeli cities (6 stations)	2006	NO_2 columns based on surface air NO_2 obs.[1]	Moderate agreement ($r = 0.6$), insignificant bias.	
Hains et al. (2009)	Netherlands, Gulf of Mexico	Sep 2006 Mar 2006	Ground-based and aircraft NO_2 profiles	Good agreement ($r = 0.8$–0.9), OMI biased high by 0–40%	Implement OMI surface albedo database
Huijnen et al. (2009)	Northwestern Europe	2008–2009	Regional air quality models, surface air NO_2 measurements	Good agreement ($r = 0.8$), OMI biased high by 0–40%	Evaluate TM4 NO_2 profiles
Lamsal et al. (2009)	Southeastern US	2005–2006	Surface air NO_2 measurements	Good agreement, OMI biased high by 0–40%	Evaluate TM4 NO_2 profiles and destriping
Zhou et al. (2009)	Switzerland and Po Valley (35 stations)	2006–2007	NO_2 columns based on surface air NO_2 obs.[2]	Good agreement ($r = 0.6$–0.8), OMI biased high by 0–60%	Implement high resolution terrain height database
Zhou et al. (2010)	Europe	2006–2007	Not available	Choice of albedo set more important than accounting for BRDF effects	Implement OMI surface albedo dataset
Zyrichidou et al. (2009)	Southeastern Europe (6 stations)	2004–2008	Surface air NO_2 observations	Moderate agreement ($r = 0.6$)	

[1] NO_2 columns based on extrapolating observed surface air NO_2 concentration throughout the depth of the boundary layer (from a local climatology).

[2] NO_2 columns based on extrapolating observed surface air NO_2 concentration throughout the depth of the boundary layer (from TM4).

AMTD
4, 2329–2388, 2011

Table 2. Summary of individual changes in regional tropospheric NO_2 retrievals relative to DOMINO v1.02. v2.0 refers to the combined effect of all individual changes.

Region[1]	Improved LUT	Improved terrain height	OMI surface albedo	Profile shape	Across-track variability	v2.0
North America (Jan. 2005)	−20%	−0.6%	+3%	−1%	+0.1%	−18.9%
Europe	−20%	+0.7%	+9%	−2%	−0.1%	−11.3%
Eastern Asia	−17%	+0.9%	−5%	−4%	−0.1%	−13.9%
Pacific	$+0.02 \times 10^{15}$ molec cm^{-2}	n.a.	-0.02×10^{15} molec cm^{-2}	n.a.	n.a.	-0.03×10^{15} molec cm^{-2}
North America (Jul. 2005)	−7%	−0.8%	−2%	−6%	−0.3%	−12.4%
Europe	−8%	−0.2%	−0.3%	−6%	−0.1%	−8.2%
Eastern Asia	−10%	−0.4%	+3%	−4%	−0.4%	−8.1%
Pacific	-0.02×10^{15} molec cm^{-2}	n.a.	n.a.	n.a.	n.a.	-0.02×10^{15} molec cm^{-2}

[1]North America defined as region between 35°–45° N, and 100°–75° W. Europe: 40°–55° N, 5° W–20° E, eastern Asia: 30°–45° N, 110° E–140° E, Pacific: 40°–0° S, 160°–110° W.

AMTD
4, 2329–2388, 2011

Table 3. Summary of individual changes in local (1° × 1°) tropospheric NO_2 retrievals relative to DOMINO v1.02. v2.0 refers to the combined effect of all individual changes.

Region[1]	Improved LUT	Improved terrain height	OMI surface albedo	Profile shape	Across-track variability	v2.0
Los Angeles (January 2005)	−40%	−4%	−14%	−1%	+0.5%	−38.7%
Po Valley	−29%	+12%	+10%	−3%	<0.1%	+8.9%
Beijing	−26%	+14%	−20%	−5%	+0.1%	−2.7%
Los Angeles (July 2005)	−19%	−4%	−15%	−4%	+0.3%	−30.1%
Po Valley	−9%	+3%	−6%	−8%	+1.3%	−14.1%
Beijing	−15%	+2%	+7%	−7%	−0.3%	−5.3%

[1]Los Angeles defined as 1° × 1° box centered at 34° N, and 118° W. Po Valley: 45° N, 9° E, Beijing: 40° N, 116.5° E.

AMTD
4, 2329–2388, 2011

Table 4. Comparison of OMI and TOMS/GOME surface albedo climatologies.

	Mean difference (440 nm) (OMI-TOMS/GOME)	Standard deviation (440 nm)	Mean difference (477 nm) (OMI-TOMS/GOME)	Standard deviation (477 nm)
January 2005	+0.0002	0.012	−0.001	0.010
July 2005	−0.002	0.013	+0.001	0.012

AMTD
4, 2329–2388, 2011

Table 5. Summertime aerosol correction factors, defined as the ratio of the air mass factor with and without aerosols (fine particles, SSA = 0.97), calculated with the SCIATRAN radiative transfer model for a typical summertime scenario over the eastern US. The AOT was 0.5 (at 440 nm), and the solar zenith angle 30°. The aerosol vertical profiles refer to a constant extinction from the surface up to 3 km, and to average observed (CALIPSO) and simulated (GOCART) profiles over the eastern US (see Yu et al., 2010). The assumed NO_2 profiles refer to the TM4 average shown in Fig. 13 (lower panel) for situations when MODIS AOT > 0.2, and a profile with the same verically integrated NO_2 amount, but now confined to a 1-km boundary layer.

NO_2 profile	3 km box profile	CALIPSO profile	GOCART profile
TM4 average	1.10	1.11	1.09
1 km box profile	0.99	0.99	0.97

AMTD
4, 2329–2388, 2011

Table 6. Wintertime aerosol correction factors, defined as the ratio of the AMF with and without aerosols, calculated with the SCIATRAN radiative transfer model for typical wintertime scenarios over the eastern US. The AOT was 0.15 (at 470 nm), and the solar zenith angle 50°. The vertical profiles refer to a constant extinction from the surface up to 0.5 km, and to extinction values that decrease exponentially with altitude. The assumed NO_2 profiles refer to the TM4 average shown in Fig. 13 (upper panel) for situations when MODIS AOT > 0.1.

Aerosol type	0.5 km box profile	0.5 km exp. profile	2 km box profile
Fine (SSA = 0.95)	1.13	1.11	1.01
Coarse (SSA = 0.95)	1.05	1.04	0.99

AMTD
4, 2329–2388, 2011

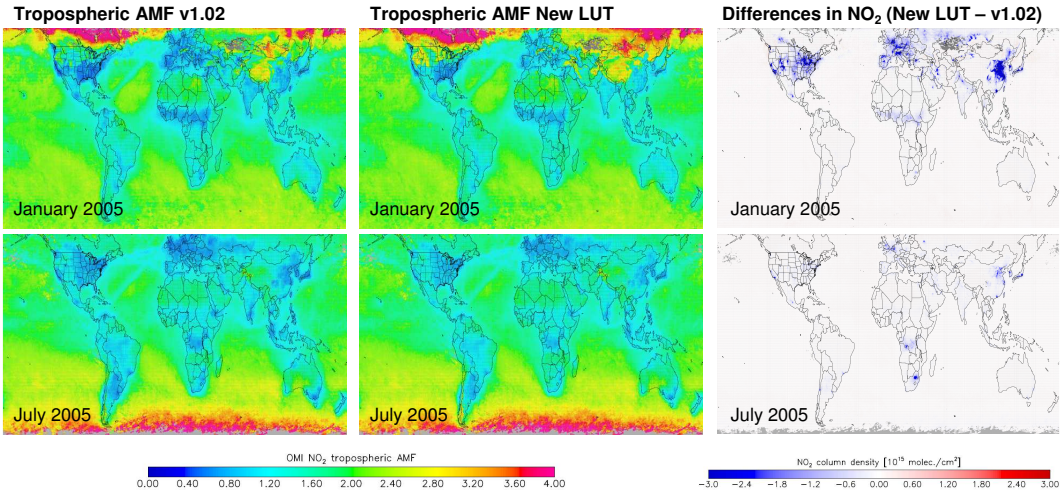

Fig. 1. Tropospheric air mass factors (AMF) calculated for v1.02 (left panels) and calculated with the new AMF lookup table (middle panels). The right panels indicate the differences between tropospheric NO_2 columns as calculated with the new AMF LUT minus tropospheric NO_2 columns calculated with the v1.02 AMF LUT. Values are monthly means for January 2005 (upper row) and July 2005 (bottom row) based on clear-sky (cloud radiance < 50%) observations.

AMTD
4, 2329–2388, 2011

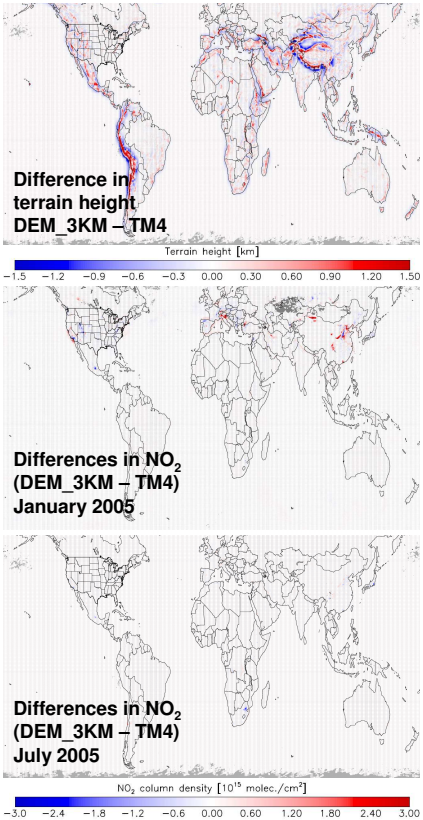

Fig. 2. Difference in terrain height calculated with the Global 3 km Digital Elevation Model data (DEM_3km, upper panel). The middle panel indicates the differences in tropospheric NO_2 columns for January 2005 as calculated with the DEM_3km terrain heights and with the coarse TM4-derived heights as in v1.02. The lower panel indicates the differences for July 2005. Values are monthly means based on clear-sky (cloud radiance < 50%) observations.

AMTD
4, 2329–2388, 2011

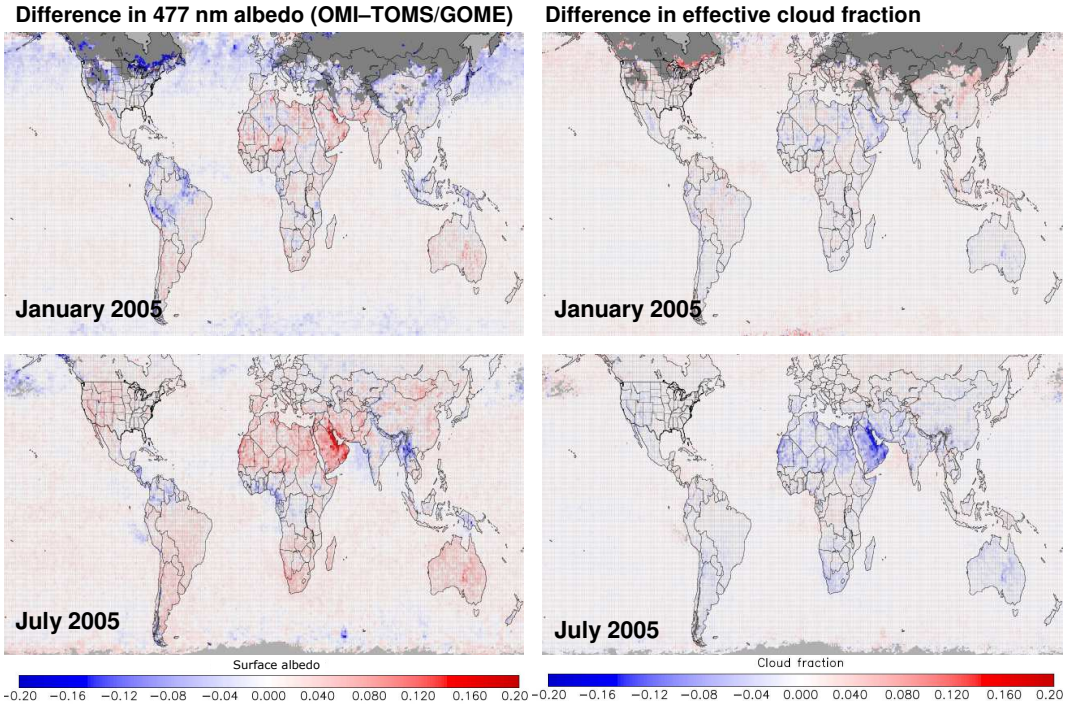

Fig. 3. Left column: difference in surface albedo between OMI (477 nm) and TOMS-GOME (479.5 nm) for monthly mean climatologies for January and July 2005. Right column: (OMI–v1.02) difference in retrieved effective cloud fractions from the O_2-O_2 algorithm calculated with different surface albedo climatologies (v1.02: TOMS-GOME, improved algorithm: Kleipool et al., 2008). Scenes with snow or ice have been excluded.

AMTD
4, 2329–2388, 2011

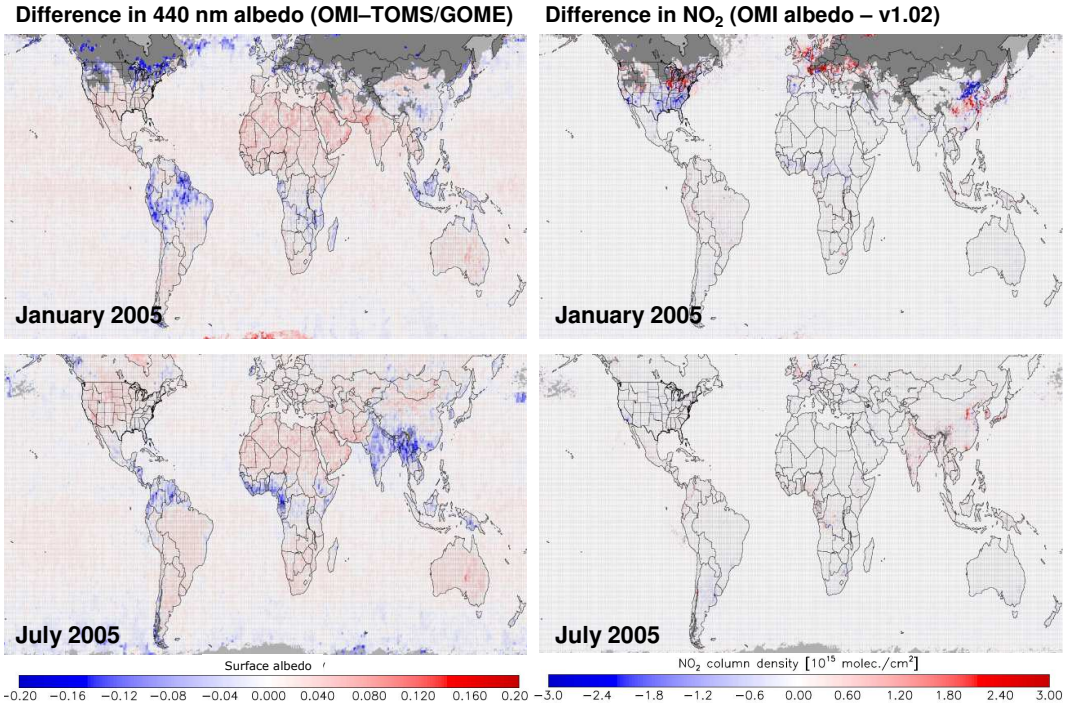

Fig. 4. Left column: difference in surface albedo between OMI and TOMS-GOME (440 nm) for January and July 2005. Right column: difference (OMI–v1.02) in retrieved tropospheric NO_2 columns from the DOMINO algorithm calculated with different surface albedo climatologies (v1.02: TOMS-GOME, improved algorithm: OMI). Only scenes with cloud radiance fractions smaller than 0.5 have been selected, and scenes with snow or ice have been excluded.

AMTD
4, 2329–2388, 2011

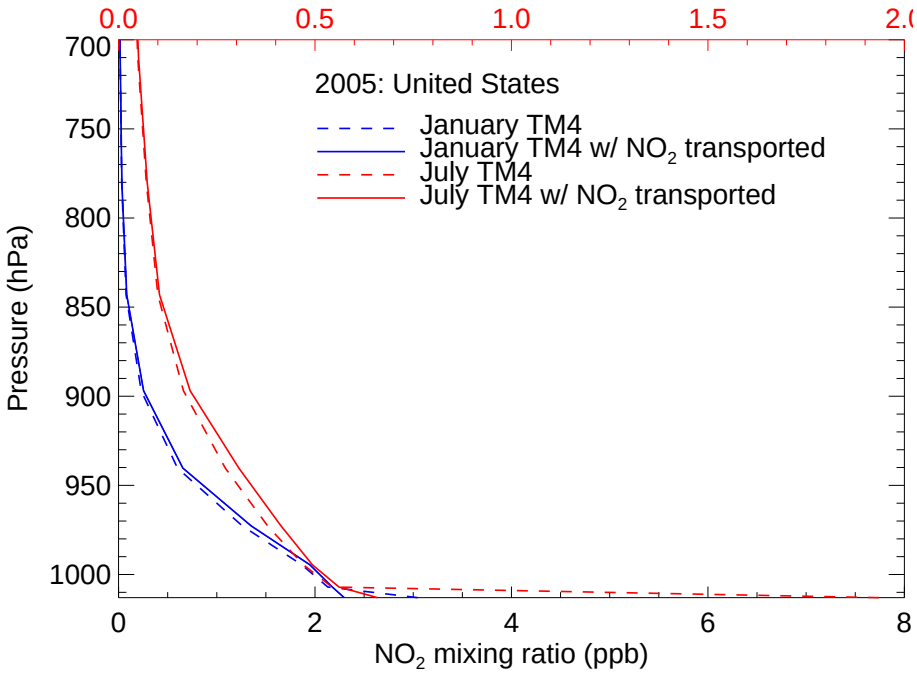

Fig. 5. Vertical profiles of NO_2 simulated with TM4 in January and July 2005. The NO_2 profiles have been sampled at 13:30 hrs local time and averaged over the US (100.5° W–76.5° W, 31° N–51° N). The dashed lines represent the original simulations as used in DOMINO v1.02 retrievals. The solid lines represent the improved simulations with NO_2 as a transported tracer in the model. The blue and red lines indicate the simulations for January and July 2005, respectively.

AMTD
4, 2329–2388, 2011

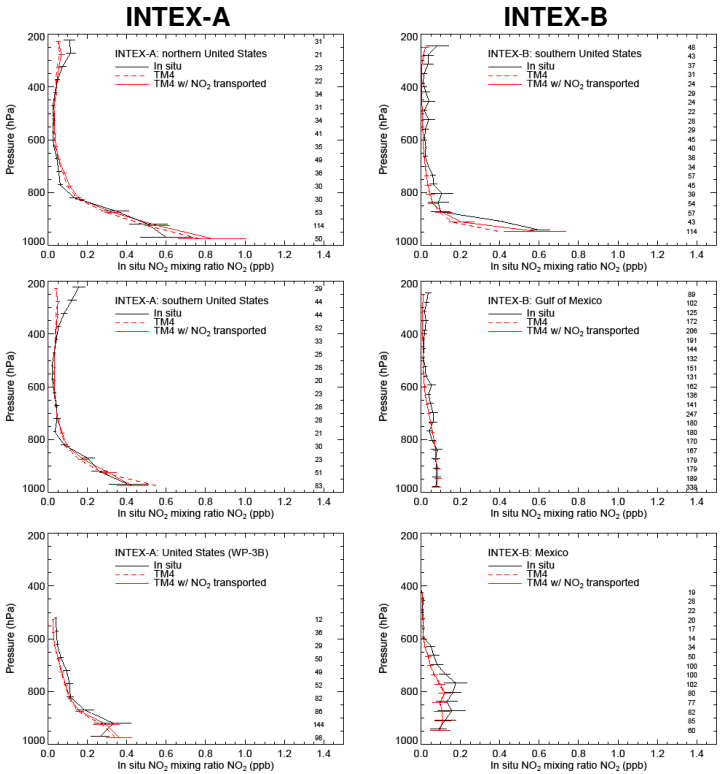

Fig. 6. Vertical profiles of NO_2 averaged over the INTEX-A/ICARTT (July–August 2004) and INTEX-B (March 2006) periods over the northern US (100° W–87°, 34° N–46° N), the southern US (100° W–87°, 28° N–34° N), the Gulf of Mexico (97° W–86°, 20° N–27° N), and Mexico (100° W–97°, 18° N–26° N) averaged over the INTEX-B period. The comparisons exclude strongly localized and recent pollution as diagnosed by $NO_x/NO_y > 0.4$ or $NO_2 < 4$ ppb. The black and red lines represent the average profiles from the in situ measurements and the TM4 model, respectively. The error bars represent the standard deviations divided by $\sqrt{n}$.

AMTD
4, 2329–2388, 2011

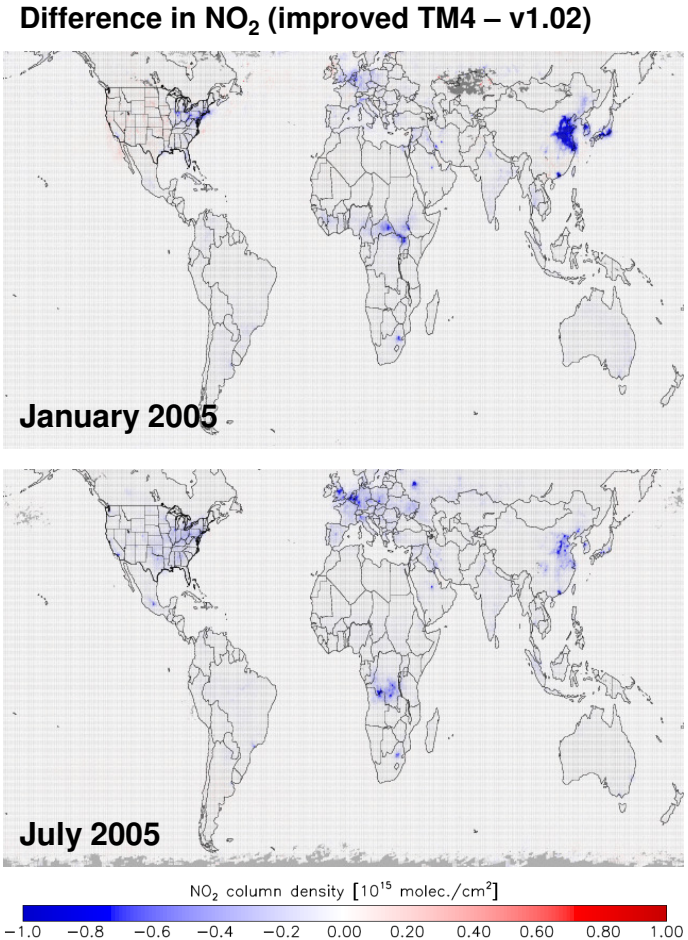

Fig. 7. Differences in retrieved OMI tropospheric NO_2 columns as calculated with the improved TM4 simulations minus v1.02. Values are monthly means for January 2005 (upper row) and July 2005 (bottom row).

AMTD
4, 2329–2388, 2011

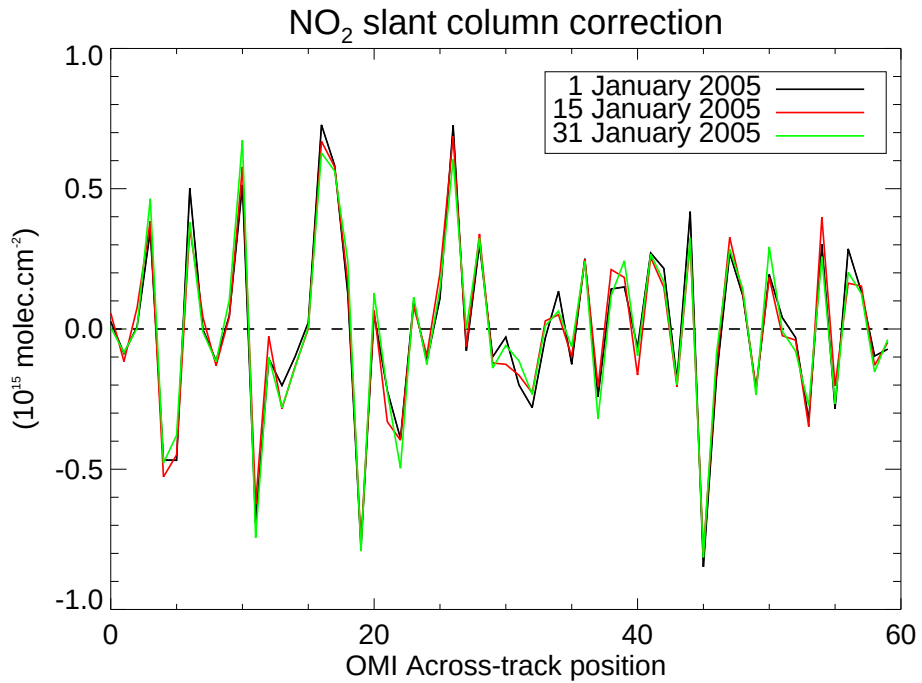

Fig. 8. OMI NO_2 slant column destriping corrections computed for three days in January 2005. The corrections represent the daily averages of 14 consecutive orbital corrections.

AMTD
4, 2329–2388, 2011

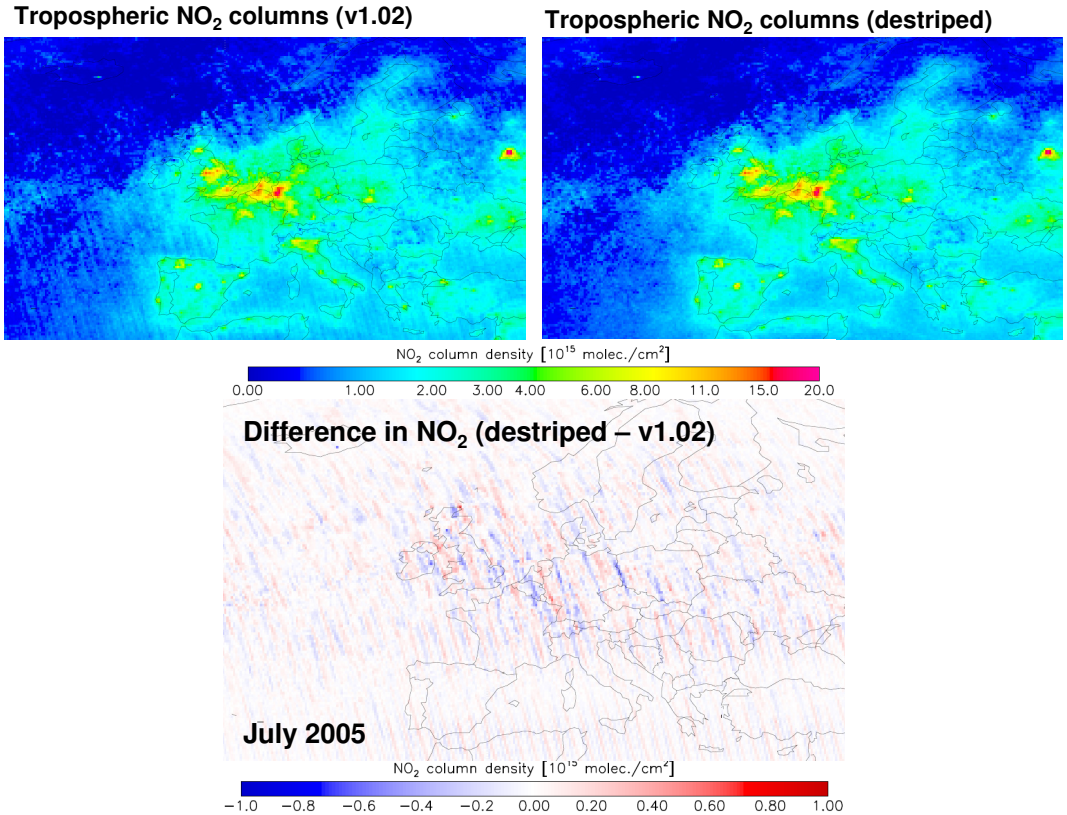

Fig. 9. Monthly mean OMI tropospheric NO_2 columns (July 2005) for v1.02 (left panel), after correction for the stripes (middle panel), and differences between destriped and original (v1.02) monthly mean OMI tropospheric columns (right panel). Cloudy scenes (cloud radiance fractions > 0.5) have been omitted in calculating the monthly mean.

AMTD
4, 2329–2388, 2011

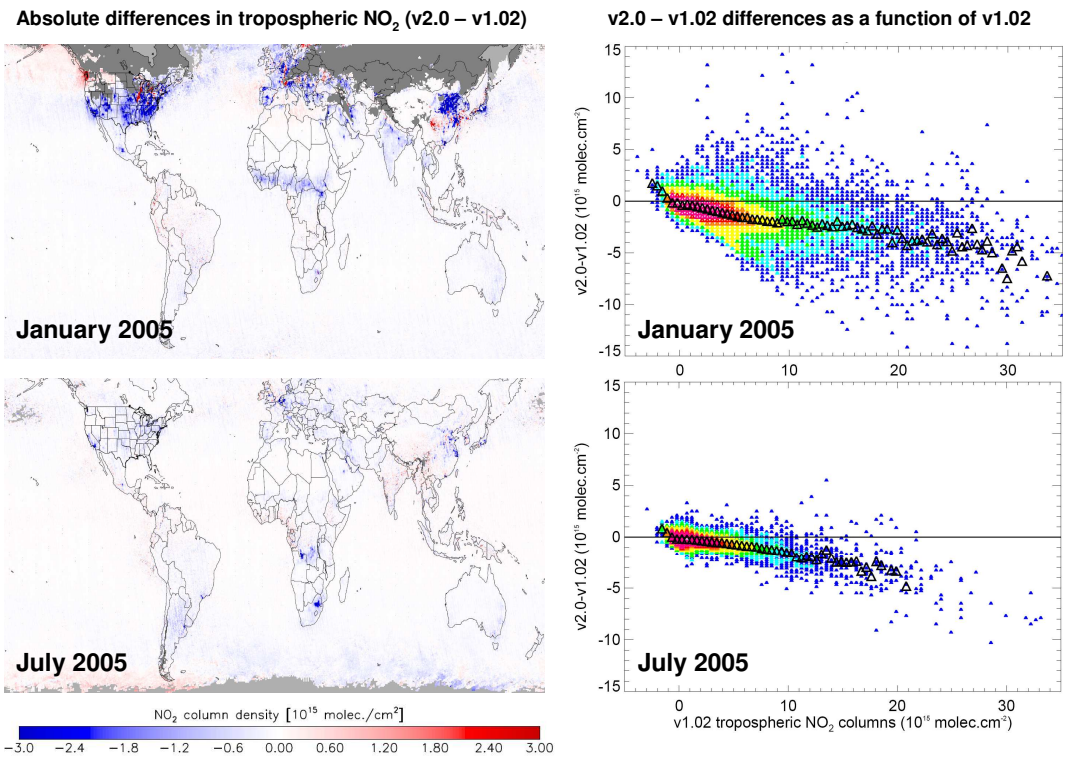

Fig. 10. Monthly average difference between v2.0 and v1.02 DOMINO tropospheric NO_2 column retrievals for January 2005 and July 2005 (left panels). Cloudy scenes (cloud radiance fractions > 0.5) have been omitted in calculating the monthly mean. The right panels show the difference between v2.0 and v1.02 as a function of the original (binned) monthly mean v1.02 values. Blue symbols indicate bins filled with 1–3 values, light blue 4–9, green 10–29, yellow 30–99, orange 100–199, red 200–399, and purple more than 400 values. The black triangles indicate the mean difference for a particular bin.

AMTD
4, 2329–2388, 2011

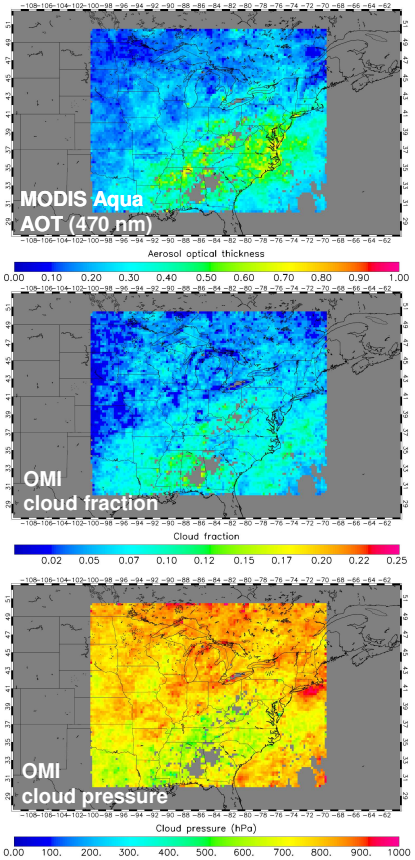

Fig. 11. Monthly average aerosol optical thickness observed from MODIS Aqua at 470 nm (upper panel), and corresponding OMI O_2-O_2 effective cloud fraction (middle panel) and effective cloud pressure (lower panel) for July 2005. Cloud fractions have been selected only for those days and locations that had a successful, cloud-free, MODIS AOT retrieval 15 min prior to the OMI observations. Grey areas indicate less than 3 successful coincidences in July 2005.

AMTD
4, 2329–2388, 2011

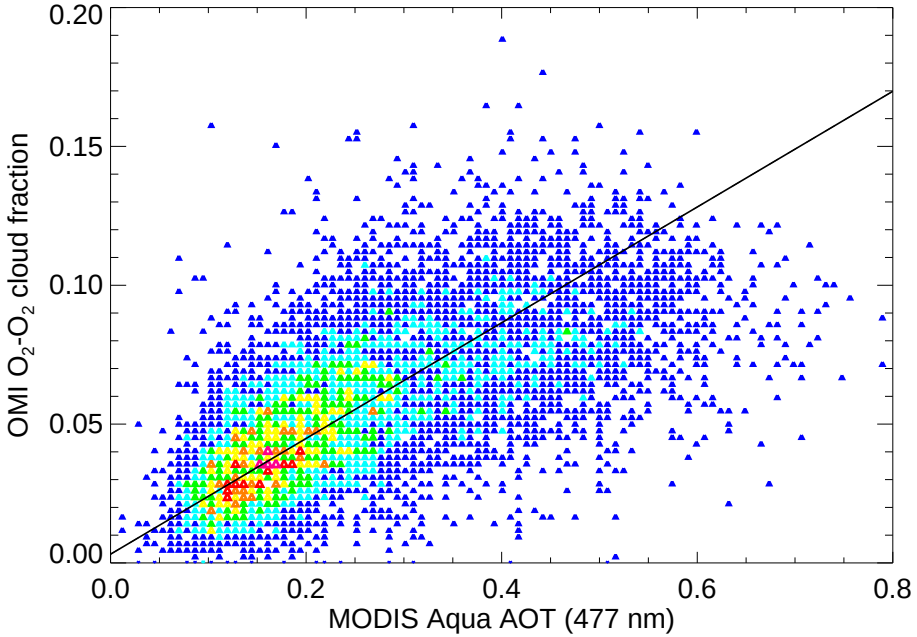

Fig. 12. Scatterplot for MODIS Aqua AOT at 470 nm (x-axis) and coinciding OMI O_2-O_2 effective cloud fractions (y-axis) observed in July 2005 (13:30 LT – local time). The colours indicate the number of times a particular grid cell has been filled, where dark blue corresponds to 1 time and red to more than 6 times. OMI effective cloud fractions can be expressed as 0.21 × AOT (reduced major axis regression). Cloud fractions have been selected only for those days and locations that had a successful, cloud-free, MODIS AOT retrieval 15 min prior to OMI.

AMTD
4, 2329–2388, 2011

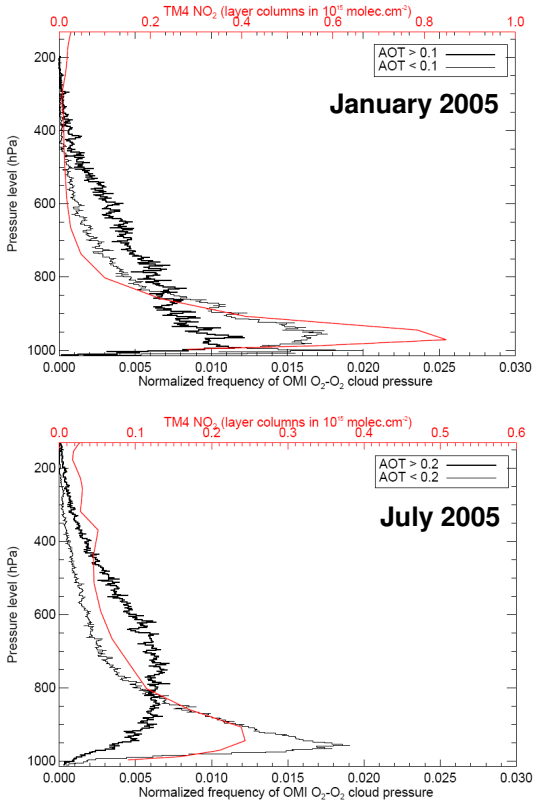

Fig. 13. Probability density functions for OMI O_2-O_2 cloud pressure levels in January 2005 (upper panel), and July 2005 (lower panel). In both panels, the pdf for the "hazy" southern US (January: MODIS > 0.1, July: MODIS > 0.2) is indicated by the thick black line, and the pdf for the clean part of the domain (January: MODIS < 0.1, July: MODIS < 0.2) has been indicated by the thin line. The red lines in both panels indicate the average vertical distribution of NO_2 (layer columns) simulated by TM4 for the "hazy" region. The upper x-axis units are in 10^{15} molec cm^{-2}.

AMTD
4, 2329–2388, 2011

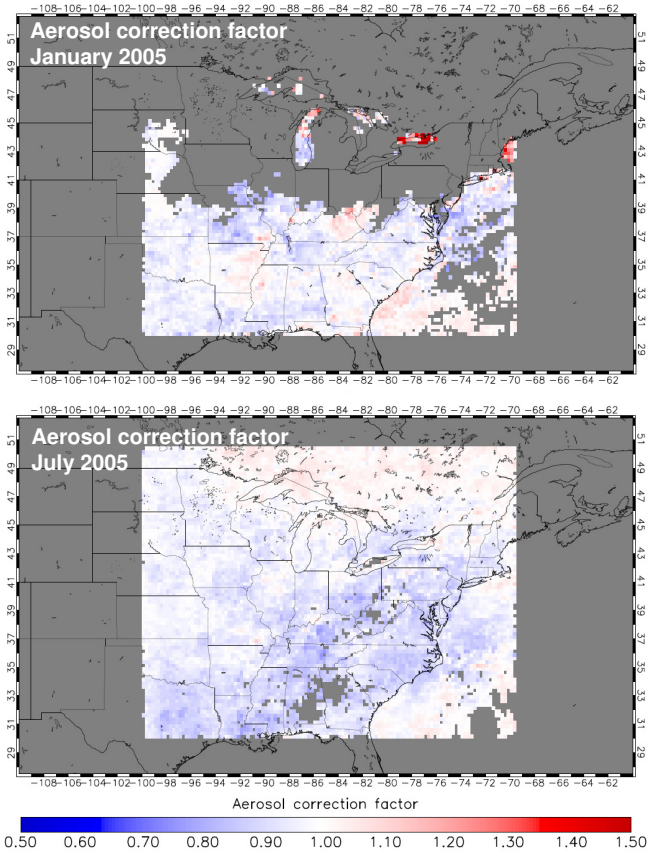

Fig. 14. Monthly average aerosol correction factor for January 2005 (upper panel) and July 2005 (lower panel). The aerosol correction factor was calculated as the ratio of the tropospheric AMF as used in the DOMINO v1.02 retrieval to the clear-sky AMF (i.e. M/M_{cr}, see Eq. 2). The aerosol correction factor was calculated only for those days and locations that had a successful, cloud-free, MODIS AOT retrieval 15 min prior to OMI. Grey areas indicate less than 3 successful coincidences in July 2005.

AMTD
4, 2329–2388, 2011

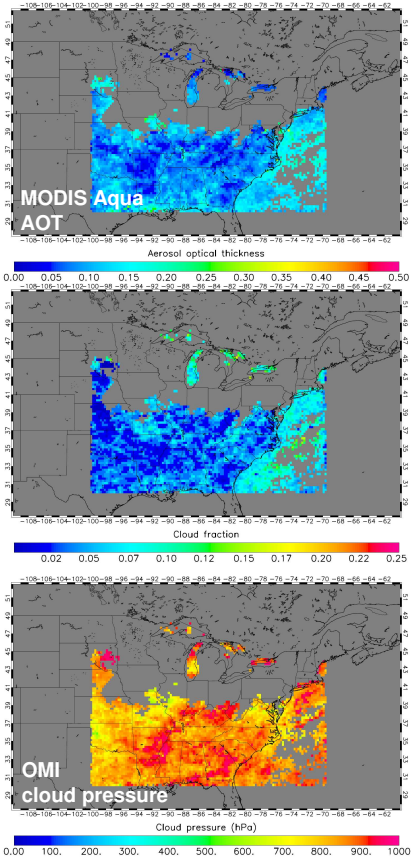

Fig. 15. Monthly average aerosol optical thickness observed from MODIS Aqua (upper panel), and corresponding OMI O_2-O_2 effective cloud fraction (middle panel) and effective cloud pressure (lower panel) for January 2005. Cloud fractions have been selected only for those days and locations that had a successful, cloud-free, MODIS AOT retrieval 15 min prior to OMI. Grey areas indicate less than 3 successful coincidences in January 2005.

AMTD
4, 2329–2388, 2011